

Anomaly Induced Domain Formation of Disoriented Chiral Condensates

Masayuki Asakawa*

Department of Physics, School of Science, Nagoya University

Nagoya, 464-8602, Japan

and

Institute for Nuclear Theory, University of Washington

Seattle, WA 98195-1550, U.S.A

Hisakazu Minakata†

Department of Physics, Tokyo Metropolitan University

Minami-Osawa, Hachioji, Tokyo 192-0397, Japan

Berndt Müller‡

Department of Physics, Duke University

Durham, NC 27708-0305, U.S.A.

(May 1, 1998)

Abstract

We discuss the effect of chiral anomaly as a possible mechanism for triggering formation of domains of disoriented chiral condensate (DCC) in relativistic heavy ion collisions. The anomalous $\pi^0 \rightarrow 2\gamma$ coupling and the strong, Lorentz

*yuki@nuc-th.phys.nagoya-u.ac.jp

†minakata@phys.metro-u.ac.jp

‡muller@phy.duke.edu

contracted electromagnetic fields of the heavy ions combine to produce the “anomaly kick” to the field configuration of the neutral pion field. We implement the effect of anomaly kick in our numerical simulation of the linear sigma model in a schematic way which preserves its characteristic features: the effect is coherent over a large region of space but is opposite in sign above and below the ion scattering plane. We demonstrate by detailed simulations with longitudinal expansion that the DCC domain formation is dramatically enhanced by the anomaly kick in spite of its small absolute magnitude. We examine the behavior of various physical quantities such as pion fields, the axial vector currents, and their correlation functions. Our results also provide useful insight into the mechanism and properties of DCC domain formation, in general. Finally, we discuss some experimental observables which can signal the anomaly induced formation of DCC.

PACS: 25.75.-q,12.38Mh,11.30.Rd

I. INTRODUCTION

One expects, on account of universality arguments, that quantum chromodynamics (QCD) with two massless quark flavors exhibits a second-order phase transition between a low-temperature phase, which shows spontaneous chiral symmetry breaking, and a chirally symmetric high-temperature phase [1,2]. The fate of this transition for the physical values of the u - and d -quark masses and a third semi-light quark flavor (s), is currently under intense investigation by means of numerical simulations of the lattice gauge theory. If the transition exists in the real world, e.g., in intermediate states in heavy ion collisions, an interesting phenomenon can occur: Large coherent domains of pion fields form due to the long range correlations associated with the second order phase transition. Unfortunately, it is unlikely that the second order transition persists with finite quark masses, as it is easily destroyed by a weak external magnetic field in the case of magnetization, and we do not expect that large domains form in an equilibrium situation [2].

However, it was argued by Rajagopal and Wilczek [2] that domains may be formed in energetic collisions where hot regions experience subsequent non-equilibrium evolution. They proposed an idealized quench approximation to model this non-equilibrium scenario [3]. It provides a concrete realization for the formation mechanism of large chirally misaligned domains, the disoriented chiral condensates (DCCs). Such chirally misaligned coherent pion field domains have been discussed by many authors [4] after the pioneering works [5–7] in the context of large neutral-charged pion fluctuations (Centauro events) that may have been seen in cosmic ray experiments [8].

The central question in the field, i.e., whether the DCC forms in high energy hadronic collisions, has been discussed extensively. We summarize these discussions below, and then we point out that the chiral anomaly combined with the environment of relativistic heavy ion collisions greatly enhances the possibility of formation of DCC domains.

The possibility of the formation of large DCC domains is investigated by means of numerical simulation [3,9,10] using the linear sigma model [11] as a low energy effective theory

of QCD. Among the most elaborate of these simulations, one with longitudinal expansion [10] indicates that large spatial domains of DCC can, indeed, develop for appropriate initial conditions.

Disoriented chiral domains can only form when a region of space is cooled down rapidly and chiral symmetry gets spontaneously broken sufficiently fast, so that the chiral order parameter $\langle \bar{q}q \rangle$ cannot adiabatically follow the shifting minimum of the effective potential. This is the reason for the quench scenario. To realize it, the hot debris formed in high energy hadronic collisions must somehow be cooled down quite rapidly. A one-dimensional expansion does not appear to be sufficiently fast [10,12], as is expected from the early calculation using the hydrodynamical model by Bjorken [13]. Therefore, a rapid three-dimensional expansion would be required [12,14] to drive the chiral field far enough out of equilibrium.

If the relics of such domains were observed in experiments where matter is heated above T_c , e.g., in relativistic heavy ion collisions, they would provide evidence for the existence for the chiral phase transition in QCD in non-equilibrium environments. Because the domains decay into coherent multi-pion states, they are predicted to reveal themselves in highly characteristic pionic observables. The unusual distribution of the pion charge ratio $R = N_{\pi^0}/N_{\pi}$ has been discussed extensively in the literature [3,5–7,15], and it is now the subject of active experimental investigations [16,17]. However, it has been shown that the charge ratio is useful as a sensitive signal for DCC formation only if a very small number of independent domains are formed [18,19], indicating the need for more advanced analyses. The possibilities include the wavelet analysis [19] and multiparticle correlations [15,16]. If the DCC can be described by a squeezed state [20] of the pion fields, as expected by the parametric resonance mechanism [21], some peculiar two pion correlations are expected [22].

We demonstrate in this paper that the Adler-Bell-Jackiw chiral U(1) anomaly [23] expressed as the Wess-Zumino term [24] in the linear sigma model does affect the chiral orientation of pion fields, and thereby enhances the DCC domain formation. As will be explained in the following sections, we formulate the effect of the anomaly as a “kick” to the neutral

pion fields imparted by the electromagnetic fields of colliding relativistic heavy ions [25], and then implement it into a numerical code simulating the linear sigma model [10]. We show by examining the various physical quantities such as pion fields, the axial vector currents, and their correlation functions that the anomaly kick, even with a tiny amplitude, acts as an effective trigger for the formation of the DCC domains.

Our manuscript is organized as follows. In Section II we will review relevant aspects of the dynamics of the axial anomaly interaction in relativistic nuclear collisions. In Section III we discuss various issues of our numerical calculations, in particular, the initial conditions for the chiral fields and the method used to solve the field equations. In Section IV we present and discuss our numerical results: the effect of the anomaly kick on domain formation, the space-time evolution of the vector and axial currents, the evolution of the pion correlation functions, and the pion density distributions. We summarize our results and make some suggestions for future experiments in Section V.

II. EFFECT OF CHIRAL ANOMALY IN DOMAIN FORMATION IN DCC; ANOMALY KICK

We review the discussion in Ref. [25], in which two of us raised the question of possible effects of the chiral anomaly in triggering DCC formation in heavy ion collisions. There the influence of the strong electromagnetic fields of colliding ions on the isospin orientations of fields was discussed in the framework of the linear sigma model. This is a natural question to ask because electromagnetism breaks isospin. However, an explicit one-loop computation of the effective potential in the linear sigma model reveals that the isospin orientation of the ground state is not affected by the uniform background electromagnetic fields. Moreover, it can be argued on the basis of symmetry considerations that this result remains valid for any spatially and temporally varying background electromagnetic fields. Therefore, it was apparent that no effect is expected at the one-loop level.

However, the above argument contains an interesting loophole. It is the presence of the

Wess-Zumino term which represents the effect of the chiral anomaly in the effective theory of QCD. It induces the $\pi^0 \rightarrow 2\gamma$ coupling in the Lagrangian of the linear sigma model as

$$\mathcal{L} = \frac{1}{2} \partial_\mu \vec{\phi} \partial^\mu \vec{\phi} - \frac{\lambda}{4} (|\vec{\phi}|^2 - f_\pi^2)^2 + H\sigma + \frac{\alpha}{\pi f_\pi} \vec{E} \cdot \vec{H} \pi_3, \quad (1)$$

where $\vec{\phi} = (\sigma, \vec{\pi})$. The ground state of the chiral field therefore becomes sensitive to the background electromagnetic fields through the anomaly term.

Then, what is the effect of the anomaly term on the chiral orientation of the pion fields, and in particular on the formation of DCC domains? To answer the question we first note that the equation of motion of the π_3 field is altered to

$$\dot{\Pi}_3 = \nabla^2 \pi_3 - \lambda (|\vec{\phi}|^2 - f_\pi^2) \pi_3 + \frac{\alpha}{\pi f_\pi} \vec{E} \cdot \vec{H}, \quad (2)$$

where Π_3 denotes the conjugate field of π_3 . Then, Π_3 is affected by the strong electromagnetic fields of heavy ions during a collision by the amount

$$\Delta \Pi_3 = \frac{\alpha}{\pi f_\pi} \int \vec{E} \cdot \vec{H} dt, \quad (3)$$

where we have used the fact that the displacement of $\vec{\phi}$ is negligible during the collision as its duration is quite short at RHIC and LHC [25]. If we use the point-nucleus approximation, $\vec{E} \cdot \vec{H}$ can be easily evaluated by computing the Lienard-Wiechert potential. One obtains

$$\vec{E} \cdot \vec{B} = \frac{2Z^2 e^2}{(4\pi)^2 M} \frac{\gamma^2}{R_1^3 R_2^3} (\vec{r} \cdot \vec{L}), \quad (4)$$

$$R_{1,2} = \sqrt{\gamma^2 (z \mp vt)^2 + \left(\vec{r}_\perp \mp \frac{\vec{b}}{2} \right)^2}, \quad (5)$$

where we have assumed a collision of identical nuclei with mass M and charge Z , and γ denotes the Lorentz factor in the center of mass frame, and $\vec{L} = \vec{b} \times M\vec{v}$ with impact parameter \vec{b} .

The physical picture resulting from the above computation is as follows. The colliding two heavy ions have Lorentz contracted electromagnetic fields which produce a non-vanishing $\vec{E} \cdot \vec{H}$ for scatterings with angular momenta higher than s -wave. During the collisions the

interaction region of space-time is affected by the anomaly term prior to the DCC formation. Since the collision time scale R/γ is much shorter than that of the DCC domains that may be formed in relativistic collisions, it is conceivable that it primarily affects the initial condition of the chiral fields. To visualize this effect of the anomaly term, we have introduced a term “anomaly kick” and described the effects imparted by the electromagnetic fields on the initial field configuration.

The anomaly kick has a distinct characteristic feature which should be important in detecting its experimental signature. The Π_3 field is kicked toward opposite directions in isospin space in the upper and lower half-spaces off the scattering plane, as seen in (4). A rough estimate in Ref. [25], however, indicates that the magnitude of the kick is small, $\Delta\Pi_3 \sim 0.1m_\pi^{-2}$. On the other hand, it is coherent over nuclear dimensions in each half-space. Therefore, while it was argued in Ref. [25] that the anomaly kick might produce interesting effects, it was difficult to draw definite conclusions on whether the anomaly effect enhances the domain formation of DCC.

In this paper we implement the kick to the conjugate field of the neutral pion field as an initial condition of the numerical simulation code of DCC domain formation using the linear sigma model [10].

We now elaborate the above estimate of $\Delta\Pi_3$ by taking the finite size of the nucleus into account. While our subsequent treatment will not rely on any details of the spatial and temporal dependence of $\Delta\Pi_3$, it is critical for a reliable estimate of the magnitude of the kick induced by the chiral anomaly. Also, this estimate will play a role in our discussions on the signature of the anomaly effect in DCC, which will be given in Sec. V.

For the purpose of taking account of the finiteness of the nuclei, we consider a sphere with radius R_A inside which total charge Z is uniformly distributed, as an abstract of each colliding nucleus. We assume that two of such spheres are colliding at Lorentz factor γ and impact parameter b in the center of mass frame, where each nucleus appears to be a sphere Lorentz contracted with the factor γ , or a pancake. We name the two pancake, pancake 1 and pancake 2. In this case, $\vec{E} \cdot \vec{B}$ is given as follows:

1) if \vec{r} is inside pancake 1, i.e., $R_1^2 \leq R_A^2$, and inside the pancake of nucleus 2, i.e., $R_2^2 \leq R_A^2$,

$$\vec{E} \cdot \vec{B} = \frac{2Z^2 e^2}{(4\pi)^2 M} \frac{\gamma^2}{R_A^6} (\vec{r} \cdot \vec{L}), \quad (6)$$

2) if \vec{r} is inside pancake 1 and outside pancake 2,

$$\vec{E} \cdot \vec{B} = \frac{2Z^2 e^2}{(4\pi)^2 M} \frac{\gamma^2}{R_A^3 R_2^3} (\vec{r} \cdot \vec{L}), \quad (7)$$

3) if \vec{r} is outside pancake 1 and inside pancake 2,

$$\vec{E} \cdot \vec{B} = \frac{2Z^2 e^2}{(4\pi)^2 M} \frac{\gamma^2}{R_1^3 R_A^3} (\vec{r} \cdot \vec{L}), \quad (8)$$

4) if \vec{r} is outside pancake 1 and outside pancake 2,

$$\vec{E} \cdot \vec{B} = \frac{2Z^2 e^2}{(4\pi)^2 M} \frac{\gamma^2}{R_1^3 R_2^3} (\vec{r} \cdot \vec{L}). \quad (9)$$

Using Eqs. (6) - (9), we obtain $\Delta\Pi_3 \sim 0.03m_\pi^{-2}$ in the central region of a non-central collision at RHIC, i.e., $z \sim 0$, $b \sim r_\perp \sim R_A = R(\text{Au})$, $\vec{r} \perp \vec{b}$, and $\gamma \sim 100$. The kick is substantially larger at LHC.

III. NUMERICAL CALCULATION — PRELIMINARIES

A. Initial Condition and Constraints on Fields

We have carried out numerical calculations on a lattice of 128×128 , on which we have imposed periodic boundary conditions. The lattice is assumed to extend in the transverse directions perpendicular to the collision axis. In the longitudinal direction, the chiral fields are assumed to be boost invariant as in [10]. The lattice spacing is a . To include the initial correlation, we have adopted an initial correlation length, ℓ_{corr} , which is generally larger than a . The initial fields and initial conjugate fields are set uniform within $\ell_{\text{corr}} \times \ell_{\text{corr}}$ cells and there is no inter-cell correlation. We have also carried out simulations with the quench

initial condition obtained from physically thermalized field configurations [26] and found that the result is insensitive to the details of the initial condition.

The initial condition for the conjugate fields has been paid little attention to up to now. The initial conditions for both the chiral fields and the conjugate chiral fields, however, are expected to greatly affect the time evolution of the field configuration. Thus, we first consider the problem of the initial condition for the conjugate fields.

We start with the following assumption on the chiral fields: the chiral fields can be treated statistically even in the case of the quench initial condition [3,10]. This means that even if the initial field fluctuation is small, the fields have experienced some ergodic processes during the preceding phases of the heavy ion collision.

The Hamiltonian density, $\mathcal{H}(\vec{x}, t)$, of the linear sigma model above T_c , is given by

$$\mathcal{H}(\vec{x}, t) = \frac{1}{2}|\vec{\Pi}(\vec{x}, t)|^2 + \frac{1}{2}|\nabla\vec{\phi}(\vec{x}, t)|^2 + \frac{\lambda}{4}(|\vec{\phi}(\vec{x}, t)|^2 + w^2)^2 - H\sigma, \quad (10)$$

We have replaced $-v^2$ by w^2 in order to take account of the chiral restoration in Eq. (10).

In the mean field approximation, w^2 and v^2 are related by [10,14],

$$w^2 = 3\langle\delta\phi_{\parallel}^2\rangle + \langle\delta\phi_{\perp}^2\rangle - v^2, \quad (11)$$

where $\delta\phi_{i\parallel}$ ($i = 0 - 3$) is the component of the fluctuation parallel to ϕ_i and $\delta\phi_{i\perp}$ is the orthogonal component. In (10), $\vec{\Pi}$ is the conjugate field of the $\vec{\phi}$ field and should not be confused with the pion field. Since we are assuming that initially the system is in the symmetric phase and that the effective potential is convex, the motion of the chiral fields is obviously bounded. Accordingly, the virial theorem holds,

$$\langle\Pi_i(\vec{x}, t)^2\rangle_t = \left\langle\phi_i(\vec{x}, t)\frac{\partial\mathcal{H}(\vec{x}, t)}{\partial\phi_i(\vec{x}, t)}\right\rangle_t, \quad (12)$$

where we have indicated that the average is a time average. Also note that there is no implied summation over multiple indices i in this subsection. Equation (12) leads to

$$\langle\Pi_i(\vec{x}, t)^2\rangle_t = \langle\phi_i(\vec{x}, t)(-\nabla^2 + \mu(\vec{x}, t)^2)\phi_i(\vec{x}, t)\rangle_t, \quad (13)$$

with

$$\mu(\vec{x}, t)^2 = \lambda(|\vec{\phi}(\vec{x}, t)|^2 + w^2). \quad (14)$$

We have neglected a term proportional to H in (13).

In numerical calculation, the Laplacian is discretized, and this affects the virial theorem, (13). In both of the methods used in our numerical calculations we shall discuss in the next subsection, the second derivative in the spatial directions is discretized by

$$\nabla_i^2 f(\vec{x}) = \frac{f(\vec{x} + a\vec{n}_i) + f(\vec{x} - a\vec{n}_i) - 2f(\vec{x})}{a^2}, \quad (15)$$

where \vec{n}_i is the unit vector in the i -th direction. For the correlation length $\ell_{\text{corr}} = 2a$, we find

$$\langle \phi_i(\vec{x}, t) \nabla^2 \phi_i(\vec{x}, t) \rangle_t = -\frac{D}{a^2} \langle \phi_i(\vec{x}, t)^2 \rangle_t, \quad (16)$$

where D is the spatial dimension, and the virial theorem becomes

$$\begin{aligned} \langle \Pi_i(\vec{x}, t)^2 \rangle_t &= \left(\frac{D}{a^2} + \mu^2 \right) \langle \phi_i(\vec{x}, t)^2 \rangle_t \\ &\approx \frac{D}{a^2} \langle \phi_i(\vec{x}, t)^2 \rangle_t. \end{aligned} \quad (17)$$

We assume that the field fluctuations at the initial time also satisfy the spatial analog of (17),

$$\langle \Pi_i(\vec{x}, t)^2 \rangle_{\text{cell}} \approx \frac{D}{a^2} \langle \phi_i(\vec{x}, t)^2 \rangle_{\text{cell}}, \quad (18)$$

where the average is taken over uncorrelated cells and events. We use the value $\ell_{\text{corr}} = 2a$ in our numerical simulations throughout this paper.

B. Computational Procedure

We have solved the equations of motion with the initial condition discussed in the previous subsection. In numerical calculation, the equations of motion are discretized. It is well-known that naively discretized partial differential equations can be numerically highly unstable, even if the underlying original continuum version of the equations is stable. On

the other hand, what is essential in the time evolution of DCC domains is the amplification of low momentum modes, or in other words, the physical instability. Thus, we have to satisfy the following two apparently contradictory requirements in solving the equations of motion on discretized lattice at the same time: eliminate unphysical instabilities, but retain the physical ones. In order to achieve this goal, algorithms such as the Lax method and leap-frog method are often adopted. However, such algorithms introduce quite often numerical viscosity. As a result, unwanted spurious suppression of fluctuations of short wave lengths occurs. This does not cause a practical problem provided that the lattice spacing is small enough compared to the typical scale of the spatial variation of the fields. In the simulation of the formation of DCC domains, however, the behavior matters because the fluctuations of short wave lengths are responsible for the change in the effective potential [10] and they affect the phase transition. Therefore, it is crucially important to keep short-range fluctuations to discuss the time evolution of DCC domains.

In order to satisfy these requirements, we have used the following two methods, (i) the first order Adams-Bashforth method [27] and (ii) the staggered leapfrog method for the second order term and the Crank-Nicholson method for the first order term in time [28]. Since (ii) is described in [28], we briefly explain (i) here. Detailed discussions on the numerical calculations will be presented elsewhere [26]. In both methods, if the lattice spacing is the same for all the spatial directions, the Laplacian is discretized as

$$\begin{aligned} \Delta f(x_i, y_j, \tau_n) \rightarrow & (f(x_{i+1}, y_j, \tau_n) + f(x_{i-1}, y_j, \tau_n) \\ & + f(x_i, y_{j+1}, \tau_n) + f(x_i, y_{j-1}, \tau_n) - 4f(x_i, y_j, \tau_n))/a^2, \end{aligned} \quad (19)$$

where τ is the proper time defined by $\sqrt{t^2 - z^2}$. Note that only the two dimensional Laplacian appears in the equations of motion since we have assumed the longitudinal boost invariance [10,13]. The difference is in how to carry out the time integration. In the Adams-Bashforth method, the increment of f , $f(x_i, y_j, \tau_{n+1}) - f(x_i, y_j, \tau_n)$, is given by [29]

$$f(x_i, y_j, \tau_{n+1}) - f(x_i, y_j, \tau_n) = \Delta\tau(\dot{f}(x_i, y_j, \tau_n) + \frac{1}{2} \nabla \dot{f}(x_i, y_j, \tau_n) + \frac{5}{12} \nabla^2 \dot{f}(x_i, y_j, \tau_n))$$

$$+\frac{3}{8} \nabla^3 \dot{f}(x_i, y_j, \tau_n) + \frac{251}{720} \nabla^4 \dot{f}(x_i, y_j, \tau_n) + \dots), \quad (20)$$

where $\Delta\tau$ is the increment in τ , $\dot{f}(x_i, y_j, \tau_n)$ is the proper time derivative of $f(x_i, y_j, \tau_n)$, and ∇^k is the backward difference operator defined by

$$\begin{aligned} \nabla g(x_i, y_j, \tau_n) &= g(x_i, y_j, \tau_n) - g(x_i, y_j, \tau_{n-1}), \\ \nabla^{k+1} g(x_i, y_j, \tau_n) &= \nabla(\nabla^k g(x_i, y_j, \tau_n) - \nabla^k g(x_i, y_j, \tau_{n-1})). \end{aligned} \quad (21)$$

The time integrals of $\sigma(x_i, y_j, \tau_n)$, $\dot{\sigma}(x_i, y_j, \tau_n)$, $\vec{\pi}(x_i, y_j, \tau_n)$, and $\vec{\dot{\pi}}(x_i, y_j, \tau_n)$ are calculated at each lattice site with the help of (20). In order to achieve satisfactory suppression of the unphysical instability, it is necessary to use sufficiently small $\Delta\tau$. For the typical parameters for the lattice spacing, the initial field fluctuation, and so on, which we shall specify shortly, we have found that $\Delta\tau$ needs to be at least 1/1800 fm or smaller. We have found that the first order Adams-Bashforth method, which uses the first two terms in the series on the RHS of Eq. (20), is good enough to suppress the unphysical instability. In the following calculations, we adopt the above value for $\Delta\tau$. We have also found that the required fineness of $\Delta\tau$ in the method (ii) is similar and have verified that the two methods give similar results.

IV. NUMERICAL CALCULATION — RESULTS AND DISCUSSIONS

A. Parameters

In the following calculations, we shall use $\lambda = 19.97$, $v = 87.4$ MeV, and $H = (119 \text{ MeV})^3$. These values correspond to the pion mass $m_\pi = 135$ MeV, the sigma mass $m_\sigma = 600$ MeV, and the pion decay constant $f_\pi = 92.5$ MeV at $T = 0$. We have assumed the longitudinal boost invariance [13] at the initial time τ_0 , which is fixed at 1 fm, and we have fixed the lattice spacing $a = 0.25$ fm throughout the calculations. The initial ϕ^i and $\dot{\phi}^i$ [30] fields in each correlated cell are randomly distributed according to a Gaussian form. In order to take account of the finiteness of the initial hot system in the transverse directions, we have adopted the following Gaussian noise parameters:

$$\begin{aligned}
\langle \sigma \rangle &= (1 - f(r))f_\pi, \\
\langle \pi_i \rangle &= 0, \\
\langle \sigma^2 \rangle - \langle \sigma \rangle^2 &= \langle \pi_i^2 \rangle = \delta_0^2 f(r), \\
\langle \dot{\sigma} \rangle &= \langle \dot{\pi}_1 \rangle = \langle \dot{\pi}_2 \rangle = 0, \\
\langle \dot{\pi}_3 \rangle &= \text{sgn}(y)a_n m_\pi^2 f(r), \\
\langle \dot{\sigma}^2 \rangle &= \langle \dot{\pi}_i^2 \rangle = \frac{D\delta_0^2}{a^2} f(r),
\end{aligned} \tag{22}$$

where r is the distance from the origin to the center of a correlated cell and δ_0^2 is a constant. In the following calculations, we use $\delta_0^2 = v^2/16$, which corresponds to the quench scenario defined in [10]. In relating $\langle \dot{\sigma}^2 \rangle$ and $\langle \dot{\pi}_i^2 \rangle$ to $\langle \sigma^2 \rangle$ and $\langle \pi_i^2 \rangle$, we have taken advantage of the virial theorem (18). $f(r)$ is an interpolation function defined by

$$f(r) = \left[\exp\left(\frac{r - R_0}{\Gamma}\right) + 1 \right]^{-1} \tag{23}$$

and describes the boundary condition. R_0 is the radius of the initially excited region where fluctuations of the classical chiral fields exist and the mean fields are different from their values in the vacuum. Outside this region, the chiral fields take the vacuum configuration, $(f_\pi, \vec{0})$. Γ is the thickness of the transient region. The results presented in this paper are obtained with $\Gamma = 0.5$ fm. a_n has been introduced to take account of the effect of the anomaly kick discussed in Section II. a_n is, in principle, dependent on the transverse coordinate. We, however, assume that it is a constant in order to concentrate on the effect of the kick to the time evolution of the system. Thus, the initial $\dot{\pi}_3$ field consists of two parts, a randomly fluctuating part and a part with global coherence. In Eq. (22), we have defined y direction to be perpendicular to the scattering plane. Following the estimate in Sec. II, we shall take $a_n = 0.1$ in the calculation, which is of similar order but a bit larger than the one expected at RHIC, but much smaller than the one expected at LHC. We note that this value is quite a moderate one as we see in the next subsection.

B. Results I — Effect of the Kick

In Figs. 1 and 2, we show an example of initial $\dot{\pi}_3$ and $\dot{\pi}_2$ field configurations, respectively. The x axis is parallel to the scattering plane, and perpendicular to the collision axis which is taken along the z direction. In this and the following calculations, we assume that the system extends infinitely in the transverse directions, i.e., $R_0 = \infty$, unless otherwise specified. With $a_n = 0.1$ it is almost impossible to recognize the embedded coherent kick, $\langle \dot{\pi}_3 \rangle = \text{sgn}(y)a_n m_\pi^2$ in Eq. (22), in the configuration of the $\dot{\pi}_3$ field. In Fig. 3, we show another initial configuration of $\dot{\pi}_3$, where the value of the kick has been artificially increased by a factor of five to $a_n = 0.5$. It is only for illustrative purpose; if the value of a_n were that large, it would be possible to distinguish the initial configurations of $\dot{\pi}_2$ and $\dot{\pi}_3$. However, such a large value of a_n is not what is suggested by the real world at least at RHIC, and the value we use in our simulations is $a_n = 0.1$.

At a glance of Figs. 1 and 2, it appears that the effect of the anomaly kick may be too tiny to be observable. However, two of us argued in Ref. [25] that it might produce non-negligible effects on the evolution of the system because it is coherent over the nuclear dimensions. Moreover, the equations of motion for the chiral fields are coupled and highly non-linear, and therefore developing the physical intuition out of them would be quite difficult. Thus, we have decided to simulate the system numerically to uncover the time evolution of the π_2 and π_3 fields with the initial conjugate field configurations with the effect of the anomaly kick. It appears to the authors that it is the only tractable way of answering to the question of how the anomaly kick is effective in triggering DCC domains.

The result we obtained is quite an unexpected one; the effect turns out to be significant. We show the proper time evolution of π_3 and π_2 , respectively, in Figs. 4 and 5 every 3 fm from τ_0 in an event. Fig. 4 indicates that the small kick results in very prominent asymmetry of the π_3 field between the upper and lower half-spaces. On the other hand, as is shown in Fig. 5, the π_2 field does not show any upper-lower space asymmetry in the course of the time evolution. We have also carried out calculation with $a_n = 0$ and have found that the

time evolution of the π_2 field is not affected by changing the value of a_n [31]. Thus, the motion of different isospin components of pion fields effectively decouples from each other, and the anomaly kick affects only the time evolution of π_3 . We will explain the reason for this effective decoupling below.

In addition to the existence of the upper-lower asymmetry, we find that the coherent structure which produces this asymmetry oscillates in time. The medium scale structure which both figures have in common corresponds to what is usually referred to as the DCC. Figs. 4 and 5 tell us that the anomaly kick induces a spatial structure in the π_3 field configuration which is larger than the ordinary DCC domains. This can also be observed in Figs. 6 and 7, in which we have plotted the Fourier power of π_3 and π_2 at $\tau = \tau_0 + 3 \text{ fm} = 4 \text{ fm}$, respectively. The scale is arbitrary, but the same scale has been used for Figs. 6 and 7. Note that this value of τ corresponds to the second proper time in Figs. 4 and 5. Both figures show a strong enhancement of low momentum modes, but in Fig. 6 we observe further sharp enhancement at very low momenta. The former is due to the amplification of low momentum modes in the formation of normal DCC domains first discussed in Ref. [3], and the latter is due to the asymmetric coherent collective oscillation of the π_3 field induced by the anomaly kick.

How can we understand such large effect in the time evolution of the π_3 field caused by such a small kick? The reason is twofold. First, it is because the different field modes are effectively decoupled in the quench case. The equations of motion for the fields are non-linear, but the interaction term in the action is proportional to $(\phi^i)^2(\phi^j)^2$. Thus, it is expected that in the quench case, where the fluctuation of the fields is small, the approach toward the equipartition is slow. This is a simple analog of the fact that the relaxation time is longer at lower temperatures in the kinetic theory. Accordingly, low momentum modes behave as if they were almost independent oscillators undisturbed by the rest of the system. Also, in the quench scenario, the fields are initially concentrated at the local maximum of the effective potential with little fluctuation, and so even a small kick is expected to be effective in determining the subsequent motion of the fields if it is coherent in space.

The second reason is the weak coupling of Nambu-Goldstone modes at low momenta. When there exists expansion, the field configurations approach to the chiral circle quickly and gets concentrated around the chiral circle after a very short time [3,10]. As is well-known, if the chiral fields are constrained on the chiral circle, the effective coupling among the pion fields becomes of the form of $\sim (\vec{\pi} \cdot \partial_\mu \vec{\pi})^2$. As a result, modes with small momenta are isolated from the rest of the system, and the effect of the coherent kick is not much affected by the presence of fluctuations of large momenta.

C. Results II — Currents

In the previous subsection, we have observed that the anomaly kick greatly affects the time evolution of the chiral fields. However, the field strengths themselves are not physical observables. The physical observables are currents, particle numbers, particle distributions, and so forth. In this subsection, we consider the behavior of physical currents.

The $O(4)$ sigma model possesses an $SU(2) \times SU(2)$ symmetry in the limit of $H \rightarrow 0$. Correspondingly, two current densities, the vector current density $V_\mu^i(\vec{x}, t)$ and axial current density $A_\mu^i(\vec{x}, t)$, where i and μ are isospin and Lorentz indices, respectively, are defined as [11,32]:

$$\begin{aligned} V_\mu^i(\vec{x}, t) &= \varepsilon^{ijk} \pi^j(\vec{x}, t) \partial_\mu \pi^k(\vec{x}, t), \\ A_\mu^i(\vec{x}, t) &= \pi^i(\vec{x}, t) \partial_\mu \sigma(\vec{x}, t) - \sigma(\vec{x}, t) \partial_\mu \pi^i(\vec{x}, t). \end{aligned} \quad (24)$$

They satisfy the CVC and PCAC, respectively,

$$\begin{aligned} \partial^\mu V_\mu^i(\vec{x}, t) &= 0, \\ \partial^\mu A_\mu^i(\vec{x}, t) &= H \pi^i(\vec{x}, t). \end{aligned} \quad (25)$$

In the following, we calculate averaged charge densities, i.e., the average of the zeroth component of the current densities. The average is taken separately over the upper and lower half-spaces with respect to the scattering plane. Average over events is taken also to reduce

fluctuations. Since the anomaly kick affects only the $\dot{\pi}_3$ field, its effect is expected to appear only in the averages of V_0^1 , V_0^2 , and A_0^3 . Other charges are not expected to show any upper-lower asymmetries.

In Fig. 8, we show $\langle A_0^1 \rangle_{\text{upper}}$, $\langle A_0^3 \rangle_{\text{upper}}$, and $\langle A_0^3 \rangle_{\text{lower}}$, as a function of the proper time. The average is taken over 10 events in Figs. 8 - 10. We observe that A_0^3 shows distinct upper-lower asymmetry. On the other hand, A_0^1 does not show it. This, however, does not mean that A_0^1 does not show domain structure. As is shown in Ref. [33], the low momentum modes of all the axial charges get amplified without the anomaly kick in the course of the time evolution from the quench initial condition. The reason for the lack of upper-lower asymmetry in the variable A_0^1 is the absence of such an asymmetry in the initial field configuration. In Fig. 9, $\langle V_0^1 \rangle_{\text{upper}}$ and $\langle V_0^3 \rangle_{\text{upper}}$ are shown. The vector charges do not show any asymmetry. Since the sign of the kick is fixed in our calculation, the expectation values of A_0^3 in the upper and lower half-spaces do not vanish after taking average over events.

The behaviors of $\langle A_0^1 \rangle_{\text{upper}}$, $\langle A_0^3 \rangle_{\text{upper}}$, and $\langle A_0^3 \rangle_{\text{lower}}$ are better understood by comparing them with the behaviors of $\langle \pi_1 \rangle_{\text{upper}}$, $\langle \pi_3 \rangle_{\text{upper}}$, and $\langle \pi_3 \rangle_{\text{lower}}$, which are shown in Fig. 10. By comparing Fig. 8 and Fig. 10, we find that the extrema of $\langle A_0^3 \rangle_{\text{upper}}$ and $\langle A_0^3 \rangle_{\text{lower}}$ approximately correspond to the zero points of $\langle \pi_3 \rangle_{\text{upper}}$ and $\langle \pi_3 \rangle_{\text{lower}}$. This is what is expected from PCAC, which says that

$$\partial^0 \langle A_0^3(\vec{x}, t) \rangle = H \langle \pi^3(\vec{x}, t) \rangle + \text{boundary terms.} \quad (26)$$

An alternative and consistent interpretation of the above feature is that the time evolutions of $\langle \pi_3 \rangle_{\text{upper}}$ and $\langle \pi_3 \rangle_{\text{lower}}$ are approximated by harmonic oscillations as seen from Fig. 10, and thus at the zero points $\langle \dot{\pi}_3 \rangle_{\text{upper}}$ and $\langle \dot{\pi}_3 \rangle_{\text{lower}}$ take extreme values. On the other hand, the sigma field does not receive any kick and, accordingly, does not show upper-lower asymmetry. Also, the oscillation of the sigma field is quickly damped and the sigma field approaches f_π [10,34]. From this observation and the definition of the axial currents, Eq. (24), it is thus concluded that the collective oscillation of the π_3 field induced by the kick is responsible for the upper-lower asymmetry and the oscillatory behavior of $\langle A_0^3 \rangle$.

The non-vanishing, upper-lower asymmetric, and oscillatory feature of $\langle A_0^3 \rangle$ survives even if the transverse extent of the system is finite. In Fig. 11, we show $\langle A_0^1 \rangle_{\text{upper}}$, $\langle A_0^3 \rangle_{\text{upper}}$, and $\langle A_0^3 \rangle_{\text{lower}}$, for the case with $R_0 = 5$ fm. The average is taken over all grid points with $r \leq 5$ fm and over 100 events. In this case, the amplitudes of the oscillations of $\langle A_0^3 \rangle_{\text{upper}}$ and $\langle A_0^3 \rangle_{\text{lower}}$ are smaller than in the $R_0 = \infty$ case. This is due to the reduction of the strengths of the pion fields caused by the transverse expansion.

D. Results III — Correlation Functions

In section IV B, we studied the time evolution of the chiral fields and their coherence in coordinate space visually by plotting the field strengths of the chiral fields. The best way of quantifying the coherence of fields is to calculate correlation functions. In this subsection, we study the correlation functions of the chiral fields and charges.

First, we define the correlation function $A_{ij}(\vec{r}, t)$ by

$$A_{ij}(\vec{r}, t) = \frac{1}{V} \int \pi_i(\vec{x}, t) \pi_j(\vec{x} + \vec{r}, t) d^3x - \frac{1}{V^2} \int \pi_i(\vec{x}, t) d^3x \int \pi_j(\vec{x}', t) d^3x', \quad (27)$$

where V is the volume of the system. Since the fields π_i form the basis of a triplet representation of $SU(2)$, $A_{ij}(\vec{r}, t)$ can be decomposed as [35]

$$A_{ij}(\vec{r}, t) = \delta_{ij} \mathcal{S}(\vec{r}, t) + \varepsilon_{ijk} \mathcal{V}_k(\vec{r}, t) + \mathcal{T}_{ij}(\vec{r}, t), \quad (28)$$

where $\mathcal{S}(\vec{r}, t)$, $\mathcal{V}_k(\vec{r}, t)$, and $\mathcal{T}_{ij}(\vec{r}, t)$ are given by

$$\begin{aligned} \mathcal{S}(\vec{r}, t) &= \frac{1}{3} A_{kk}(\vec{r}, t), \\ \mathcal{V}_k(\vec{r}, t) &= \frac{1}{2} \varepsilon_{ijk} A_{ij}(\vec{r}, t), \\ \mathcal{T}_{ij}(\vec{r}, t) &= \frac{1}{2} (A_{ij}(\vec{r}, t) + A_{ji}(\vec{r}, t)) - \delta_{ij} \mathcal{S}(\vec{r}, t). \end{aligned} \quad (29)$$

If $A_{ij}(\vec{r}, t) = A_{ji}(-\vec{r}, t)$ holds, $\mathcal{V}_k(\vec{r}, t)$ vanishes.

Next, let us assume a solution of the equation of motion for the π_i field, $\pi_i(\vec{x}, t)$, with given initial condition at $t = t_0$. Suppose the sign of the initial conditions for the ϕ_i and $\dot{\phi}_i$

fields is reversed, $\phi_i(\vec{x}, t_0) \rightarrow -\phi_i(\vec{x}, t_0)$, $\dot{\phi}_i(\vec{x}, t_0) \rightarrow -\dot{\phi}_i(\vec{x}, t_0)$. Then, the solution for the π_i field in this case is just $-\pi_i(\vec{x}, t)$. This is because the interaction term in the equation of motion for π_i is proportional to $(\sigma^2 + \pi_1^2 + \pi_2^2 + \pi_3^2)\pi_i$. Thus, if the probability distribution $P(\pi_k(\vec{x}), \dot{\pi}_k(\vec{x}))$ of the initial values of the fields π_k and $\dot{\pi}_k$ satisfies

$$P(\pi_k(\vec{x}), \dot{\pi}_k(\vec{x})) = P(-\pi_k(\vec{x}), -\dot{\pi}_k(\vec{x})), \quad (30)$$

the event averages of all the off-diagonal correlation functions $\langle A_{ij}(\vec{r}, t) \rangle$ vanish, and hence $\langle \mathcal{T}_{ij}(\vec{r}, t) \rangle = 0$ for $i \neq j$. In the case we are dealing with, only the $\dot{\pi}_3$ field is kicked, and for the π_1 and π_2 fields, the relationship (30) still holds. Accordingly, $\langle \mathcal{T}_{ij}(\vec{r}, t) \rangle = 0$ for $i \neq j$. We have indeed confirmed this in our numerical calculation. Hence, in the following, we shall only consider the diagonal correlation functions.

First, in Fig. 12, we show $A_{11}(r, \tau)$ at three different proper times. We have used the default parameters and the result has been obtained by averaging over 5 events. The average over the azimuthal angle of \vec{r} has been performed. We observe that the correlation function changes rather substantially as a function of the proper time. The pion fields oscillate and both the coherent part and short distance fluctuation change in time. Due to the energy conservation, when the amplitude of the coherent motion is at the maximum, the local fluctuation is at the minimum. $\tau = 5$ fm approximately corresponds to this time and in a two dimensional plot domain structure is clearly observed without fluctuations of much shorter scale.

One interesting feature of A_{11} is the oscillatory behavior. This was already observed in Ref. [10]. It has been sometimes interpreted as a sign of the shrinkage of the domains or occurrence of anti-correlation. However, this is not the correct interpretation. The behavior is actually due to the pseudo-periodicity in the distribution of the pion field strengths. This can be seen, for instance, in Fig. 5. The peaks of the pion field strength are not distributed randomly. The reason for this is traced back to the mechanism responsible for the formation of DCC domains, i.e., the amplification of low momentum pion modes. The wavelengths of the low momentum modes characterize not only the size of each domain but also the

distribution or separation of domains. In the mean field theory, modes with momentum less than a certain cutoff value are amplified at each time and not only specific modes are amplified. This is the reason why the distribution of the peaks is not utterly regular. We note that a similar oscillatory behavior in correlation functions of systems without regular lattice structure (such as liquids) is also known in condensed matter physics [36]. DCC formation is often compared to the spinodal decomposition observed in glass and metal [37,38]. It is known, however, that in the case of the spinodal decomposition only modes in a small range of momenta are selectively amplified with large amplification factors. As a result, the distribution of domains created by the spinodal decomposition generally shows more periodic structure.

Next, we show $A_{33}(r, \tau)$ at $\tau = 7$ and 9 fm in Fig. 13. As we have seen that the time evolution of the π_3 field is asymmetric between the upper and lower half-spaces, we distinguish the same side and different side correlation functions, $A_{33}^{++}(r, \tau)$ and $A_{33}^{+-}(r, \tau)$. They are defined as follows:

$$\begin{aligned} A_{33}^{++}(r, \tau) &= \langle (\pi_3(i, \tau) - \langle \pi_3(\tau) \rangle) (\pi_3(j, \tau) - \langle \pi_3(\tau) \rangle) \rangle_{ij} \quad \text{sgn } y(i) \text{sgn } y(j) > 0, \\ A_{33}^{+-}(r, \tau) &= \langle (\pi_3(i, \tau) - \langle \pi_3(\tau) \rangle) (\pi_3(j, \tau) - \langle \pi_3(\tau) \rangle) \rangle_{ij} \quad \text{sgn } y(i) \text{sgn } y(j) < 0, \end{aligned} \quad (31)$$

where i and j are grid points, $\langle \dots \rangle_{ij}$ is the average over pairs of those grid points, i and j , such as the distance between them is r and the product of the signs of their y -coordinates is either positive ($++$) or negative ($+-$), and $\langle \pi_3(\tau) \rangle$ is the average of the strength of the π_3 field at τ over the whole space. We show the average of Eq. (31) over 5 events in Fig. 13. From Fig. 10, we see the amplitude of the collective motion of the π_3 field is about the maximum at $\tau = 7$ fm, and, accordingly, the upper-lower asymmetry is largest at that time. Correspondingly, we can clearly see the asymmetry in the correlation function, A_{33} at $\tau = 7$ fm. On the contrary, at $\tau = 9$ fm, there is little asymmetry observed in A_{33} . This is because, as is seen from Fig. 10, the amplitude of the coherent oscillation almost vanishes at this time. For comparison, we plot the same side and different side correlations of the π_1 field in Fig. 14 at $\tau = 7$ fm. As in the previous figures, an average over 5 events has been

taken. There is little difference between the two correlation functions. We have confirmed that this small amount of difference is solely due to statistical fluctuations by carrying out other sets of statistically independent simulations.

We have further calculated the correlation functions of the axial and vector charges. We have defined the same side and different side correlation functions of the axial charges, $B_{kl}(r, \tau)$, and the vector charges, $C_{kl}(r, \tau)$, by

$$\begin{aligned} B_{kl}(r, \tau) &= \langle (A_0^k(i, \tau) - \langle A_0^k(\tau) \rangle) (A_0^l(j, \tau) - \langle A_0^l(\tau) \rangle) \rangle_{kl}, \\ C_{kl}(r, \tau) &= \langle (V_0^k(i, \tau) - \langle V_0^k(\tau) \rangle) (V_0^l(j, \tau) - \langle V_0^l(\tau) \rangle) \rangle_{kl}, \end{aligned} \quad (32)$$

where the notations are the the same as before and the average is taken over 5 events. In Fig. 15, we show the same side and different side correlation functions of A_0^3 at $\tau = 9$ fm. We note that this proper time corresponds to when the asymmetry in A_0^3 is approximately at maximum as seen in Fig. 8. In Fig. 15, the asymmetry between the same side and different side correlation functions is observed. However, it should be noted that the degree of coherence is less than that of the field-field correlation functions. In Fig. 16, same side correlation functions of A_0^1 , V_0^1 , and V_0^3 are plotted at $\tau = 9$ fm. This indicates that A_0^1 shows some coherence, but that neither V_0^1 nor V_0^3 shows coherent behavior [33].

E. Results IV — Pion Density Distributions

It has often been argued that the pion density in coordinate space is proportional to the square of the pion field strength. This is actually the basis for the expression for the probability to have a DCC domain in which the fraction of neutral pions, $n_{\pi^0}/(n_{\pi^0} + n_{\pi^+} + n_{\pi^-})$, takes the value R [5–7],

$$P(R) = \frac{1}{2\sqrt{R}}. \quad (33)$$

In this formula, the pion fields are assumed to be static, $\dot{\pi}_i = 0$. In reality, however, the pion fields are not static and also include substantial fluctuations. When the pion

fields are not static, the pion densities depend also on the conjugate fields. This is just an analog of the one dimensional harmonic oscillator case; both the coordinate variable and its canonical conjugate (momentum) variable contribute to the energy, i.e., the number of quanta. Moreover, when the pion fields are fluctuating even classically, the definition of a domain itself is not unambiguous. However, in the following we shall calculate the local pion densities in coordinate space as a function of proper time and discuss the typical size of clusters defined by the distribution of local pion densities thus obtained.

Quantum field theory is often formulated in momentum space. Creation and annihilation operators are usually defined for momentum eigenstates. It is because the Hamiltonian for free fields reduces to the sum of those of harmonic oscillators in momentum space. However, as we have discussed above, what we need here is the pion density distribution in coordinate space. For that purpose, we first define the pion creation operators and annihilation operators in coordinate space as the Fourier transforms of those in momentum space. For example, the creation operators for π^+ , π^- , and π^0 at \vec{x} are given, respectively, by

$$\begin{aligned} a_{\pi^+}^\dagger(\vec{x}) &= \frac{1}{(2\pi)^{3/2}} \int e^{-i\vec{p}\cdot\vec{x}} \left(\sqrt{\frac{\omega_p}{2}} \pi^{+\dagger}(\vec{p}) - i \frac{1}{\sqrt{2\omega_p}} \dot{\pi}^{+\dagger}(\vec{p}) \right) d^3p, \\ a_{\pi^-}^\dagger(\vec{x}) &= \frac{1}{(2\pi)^{3/2}} \int e^{-i\vec{p}\cdot\vec{x}} \left(\sqrt{\frac{\omega_p}{2}} \pi^{-\dagger}(\vec{p}) - i \frac{1}{\sqrt{2\omega_p}} \dot{\pi}^{-\dagger}(\vec{p}) \right) d^3p, \\ a_{\pi^0}^\dagger(\vec{x}) &= \frac{1}{(2\pi)^{3/2}} \int e^{-i\vec{p}\cdot\vec{x}} \left(\sqrt{\frac{\omega_p}{2}} \pi^{0\dagger}(\vec{p}) - i \frac{1}{\sqrt{2\omega_p}} \dot{\pi}^{0\dagger}(\vec{p}) \right) d^3p, \end{aligned} \quad (34)$$

where $\omega_p = \sqrt{m_\pi^2 + \vec{p}^2}$, $\pi_i(\vec{p})$ and $\dot{\pi}_i(\vec{p})$ are, respectively, the Fourier transforms of $\pi_i(\vec{x})$ and $\dot{\pi}_i(\vec{x})$. The charge eigenstate fields $\pi^+(\vec{x})$, $\pi^-(\vec{x})$, and $\pi^0(\vec{x})$ are defined as

$$\begin{aligned} \pi^\pm(\vec{x}) &= \frac{\pi_1(\vec{x}) \pm i\pi_2(\vec{x})}{\sqrt{2}}, \\ \pi^0(\vec{x}) &= \pi_3(\vec{x}). \end{aligned} \quad (35)$$

We define the local density operators for the π_i field, $n_{\pi_i}(\vec{x})$ as

$$n_{\pi_i}(\vec{x}) = a_{\pi_i}^\dagger(\vec{x}) a_{\pi_i}(\vec{x}). \quad (36)$$

We note that since

$$\pi^\pm(\vec{p}) \neq \pi^{\pm\dagger}(\vec{p}), \quad (37)$$

in general,

$$n_{\pi^+}(\vec{x}) \neq n_{\pi^-}(\vec{x}). \quad (38)$$

Thus, in principle, the electric charge density can fluctuate and can take non-zero values locally. The creation operators and density operators satisfy the following commutation relation:

$$[n_{\pi_i}(\vec{x}), a_{\pi_j}^\dagger(\vec{x}')] = \delta_{ij} \delta(\vec{x} - \vec{x}') a_{\pi_j}^\dagger(\vec{x}'). \quad (39)$$

This justifies our definition of the creation, annihilation, and density operators in coordinate space. These creation operators do not create momentum or energy eigenstates, since the position is specified. However, Parsival's relation is satisfied,

$$\int n_{\pi_i}(\vec{x}) d^3x = \int n_{\pi_i}(\vec{p}) d^3p, \quad (40)$$

and, accordingly, the integrations over coordinate space and momentum space give the same total number.

In this subsection, we have not yet specified the physical state of the system. In order to extract the coordinate space distribution of each pion species and find the typical size of DCC domains in the original sense, we first rewrite $n_{\pi_i}(\vec{x})$ as follows:

$$n_{\pi_i}(\vec{x}) = \frac{1}{2} \left| \int (P(\vec{x} - \vec{x}') \pi_i(\vec{x}') + iQ(\vec{x} - \vec{x}') \dot{\pi}_i(\vec{x}')) d^3x' \right|^2, \quad (41)$$

where $P(\vec{x})$ and $Q(\vec{x})$ are functions defined by

$$\begin{aligned} P(\vec{x}) &= \frac{1}{(2\pi)^3} \int \sqrt{\omega_p} e^{i\vec{p}\cdot\vec{x}} d^3p, \\ Q(\vec{x}) &= \frac{1}{(2\pi)^3} \int \frac{1}{\sqrt{\omega_p}} e^{i\vec{p}\cdot\vec{x}} d^3p. \end{aligned} \quad (42)$$

The non-local feature of n_{π_i} is obvious in Eq. (41). We now assume that the system is in a coherent state $|c\rangle$ and the operators $\pi(\vec{x})$ and $\dot{\pi}(\vec{x})$ in $a(\vec{x})$ operating on $|c\rangle$ can be

replaced by those values obtained in the classical simulation, $\pi_{\text{cl}}(\vec{x})$ and $\dot{\pi}_{\text{cl}}(\vec{x})$. Note that this procedure needs to be modified if the system is not in a coherent state [20]. This possibility will be considered elsewhere.

In Figs. 17 and 18, we show the distributions of π^0 and π^+ density on the x - y plane, respectively, every 3 fm from τ_0 in an event. We have used the same initial field configuration as for Figs. 4 and 5. From Figs. 17 and 18, we can clearly see the formation of domains also in this definition. However, we recognize in these figures several features different from Figs. 4 and 5. First, the distributions of π^0 and π^+ densities fluctuate more than those of the π^0 and π^+ fields themselves. This is because the definitions of π^0 and π^+ density include, respectively, $\dot{\pi}^0$ and $\dot{\pi}^+$ fields, which are not so much amplified as π^0 and π^+ fields and noisier than those. Second, the distribution of π_0 density does not show the upper-lower asymmetry. This is because the definition of $n_{\pi_i}(\vec{x})$ is quadratic in $\pi_i(\vec{x})$ and $\dot{\pi}_i(\vec{x})$. Third, after the initial formation of the large scale structure, the pattern of the distribution remains almost unchanged except for the occurrence of slight diffusion. This tells us that domains in this definition are almost frozen at fixed positions on the x - y plane. The last point is also clearly seen in Fig. 19, where we have plotted the time evolution of the distribution of $R(\vec{x}) = n_{\pi^0}(\vec{x}) / (n_{\pi^+}(\vec{x}) + n_{\pi^-}(\vec{x}) + n_{\pi^0}(\vec{x}))$ in the same event.

In Fig. 20, we have plotted R , which is defined as

$$R = \sum_{\text{event}} \int n_{\pi^0}(\vec{k}) d^3k \Big/ \sum_{\text{event}} \int (n_{\pi^+}(\vec{k}) + n_{\pi^-}(\vec{k}) + n_{\pi^0}(\vec{k})) d^3k, \quad (43)$$

where $n_{\pi_i}(\vec{k})$ is the pion density at momentum \vec{k} , in a solid line. Ten events were used in the average. The dashed line is the same except that the momentum integration is limited to $k < 250$ MeV. Fig. 20 shows striking enhancement of neutral pions, especially in the low momentum region. Note that $R = 0.375$ corresponds to $N_{\pi^0} : N_{\pi^+} : N_{\pi^-} = 1.2 : 1 : 1$ provided $N_{\pi^+} = N_{\pi^-}$. Also note that the distribution of R deviates from the celebrated form, $P(R) = 1/2\sqrt{R}$, when $\pi_i(\vec{x})$ is not uniform, and moreover that even if $\pi_i(\vec{x})$ is spatially uniform, when $\dot{\pi}_i(\vec{x}) \neq 0$, R also depends on $\dot{\pi}_i(\vec{x})$. Fig. 21 is the same as Fig. 20 except that no anomaly kick is exerted. In this case, R is, as is expected, approximately 1/3 regardless

of the cutoff in the momentum integral.

We have found that the distribution of the excess π^0 's is not isotropic in momentum space. They are distributed more in the y -direction than the x -direction. This reflects the Fourier power of the initial anomaly kick: in the $R_0 \rightarrow \infty$ limit, the Fourier power of the kick, $\text{sgn}(y)a_n m_\pi^2$, is concentrated at $p_x = 0$ in the x -direction, while it has support at $p_y \neq 0$ in the y -direction. In addition, the effect of the anomaly kick is expected to be observed more in the central rapidity region than in the fragmentation region, because the kick is created when the two colliding nuclei are almost overlapping with each other.

V. SUMMARY

In summary, we have studied the physical influence of the axial anomaly on the formation mechanism of disoriented chiral condensate domains in relativistic heavy ion collisions. Our study is based on the framework of the linear sigma model with initial conditions corresponding to a “quench” modified by a small, spatially coherent displacement (“anomaly kick”) of the conjugate field of the neutral pion field caused by the action of the electromagnetic fields of the colliding nuclei. These initial conditions correspond to a somewhat schematic, but quantitatively realistic abstraction of conditions that could arise in semiperipheral collisions of two heavy nuclei at RHIC or LHC.

We have found that the anomaly kick has practically no influence on the evolution of the charged pion fields but causes noticeable modifications to the dynamics of the neutral pion field. It produces a spatial asymmetry in the formation of DCC domains above and below the scattering plane and leads to a general enhancement of the π^0 domain structure. The up-down asymmetry is clearly expressed in the integrated $I_3 = 0$ component of the axial charge on both sides of the scattering plane. Since the signs of the pion fields or the axial charges are not directly connected with hadronic observables, this up-down asymmetry is difficult to establish experimentally.

However, the overall enhancement of domain formation in the $I_3 = 0$ direction is found to

lead to a relative increase in the neutral pion yield, raising the ratio $R = N_{\pi^0}/N_{\pi}$ significantly above the value $1/3$ dictated by isospin symmetry. This signature, which survives event averaging, should be experimentally detectable. Because it has a different characteristic than the isospin breaking due to the effects caused by charges of incident nuclei, which alters the π^+/π^- ratio, it can be discriminated from this well known effect. Also, the mechanism of isospin breaking discussed here can be distinguished from the pion mass splitting, which leads to a similar but smaller enhancement of R , because it depends on the impact parameter and vanishes for precisely central collisions.

Finally, we have analyzed spatial correlation functions of the pion field. The oscillations already observed by others appear to be caused by long-range correlations in the positions of different DCC domains. These correlations correspond to a fluid-like spatial structure of the domain locations and are clearly visible in equal-time snapshots of the chiral order parameter.

If the domain formation of DCC is in fact triggered by the anomaly effect discussed in this paper, there is a clear experimental signature which testifies for its origin; the formation rate of DCC should show a strong energy and atomic number dependences characteristic to the mechanism. The parameter a_n which measures the magnitude of the anomaly kick scales as E and Z^2 , respectively, as center of mass energy E and the atomic number Z are varied. It is tempting to speculate that the formation rate of DCC somehow should reflect these dependences.

Experimental searches for DCC formation have, so far, concentrated on central collisions between two heavy nuclei, because it is here where one expects the highest energy densities to occur over the largest spatial volumes. These two conditions are important, because matter needs to be heated above T_c over a large volume if one wants to observe the characteristic effects of a phase transition.

However, our results indicate that semi-peripheral collisions, i.e., collisions with an impact parameter $b \sim R_A$, may be even more favorable for DCC formation. Two reasons contribute to this phenomenon: (1) The expansion time scale is generally shorter in periph-

eral collisions than in central ones, and a three-dimensional expansion may occur more easily in non-central collisions, leading to the quench initial condition. (2) Collisions of heavy nuclei with $b \neq 0$ produce the “anomaly kick”, which favors the formation of large uniform domains of the quark condensate by inducing a collective motion in the direction of the neutral pion field. Therefore, we suggest that the search for DCC formation in relativistic heavy ion collisions at RHIC should not be confined to central collisions only.

ACKNOWLEDGMENTS

We thank Krishna Rajagopal for many valuable communications and for sharing with us useful knowledges through the collaboration on the work [33]. M. A. and H. M. would like to thank for warm hospitality at Duke University, and M. A. and B. M. extend their gratitude to the members of Physics Department at Tokyo Metropolitan University for warm hospitality and fruitful discussions. M. A. wishes to thank the Institute for Nuclear Theory at the University of Washington for its hospitality during his stay. This research has been supported in part by the U.S. Department of Energy under Grant DE-FG02-96ER40945. H. M. is partly supported by Grant-in-Aid for Scientific Research no. 09640370 of the Japanese Ministry of Education, Science and Culture, and by Grant-in-Aid for Scientific Research no. 09045036 under the International Scientific Research Program, Inter-University Cooperative Research.

REFERENCES

- [1] R. D. Pisarski and F. Wilczek, Phys. Rev. D **29** (1984) 338.
- [2] K. Rajagopal and F. Wilczek, Nucl. Phys. **B399** (1993) 395.
- [3] K. Rajagopal and F. Wilczek, Nucl. Phys. **B404** (1993) 577.
- [4] For a review, see: K. Rajagopal, in: Hwa, R.C. (ed.): *Quark-Gluon Plasma*, vol. 2, p. 484.
- [5] A. A. Anselm and M. G. Ryskin, Phys. Lett. **B266** (1991) 482.
- [6] J. D. Bjorken, K. L. Kowalski, and C. C. Taylor, SLAC Report No. SLAC-PUB-6109.
- [7] J. -P. Blaizot and A. Krzywicki, Phys. Rev. D **46** (1992) 246.
- [8] L. T. Baradzei et al., Nucl. Phys. **B370** (1992) 365. J. Lord and J. Iwai, paper submitted to International Conference on High Energy Physics, Dallas, Texas, 1992.
- [9] S. Gavin, A. Gocksh, and R. D. Pisarski, Phys. Rev. Lett. **72** (1994) 2143.
- [10] M. Asakawa, Z. Huang, and X. N. Wang, Phys. Rev. Lett. **74** (1995) 3126.
- [11] M. Gell-Mann and M. Levy, Nuovo Comento **16** (1960) 705.
- [12] J. Randrup, Phys. Rev. Lett. **77** (1996) 1226.
- [13] J. D. Bjorken, Phys. Rev. D **27** (1983) 140.
- [14] S. Gavin and B. Müller, Phys. Lett. **B329** (1994) 486.
- [15] C. Greiner, C. Gong, and B. Müller, Phys. Lett. **B316** (1993) 226.
- [16] T. Brooks et al. (MiniMax Collaboration), hep-ph/9609375. J. Street, Talk at Argonne Workshop on Hadron Systems at High Density and/or High Temperature, August 7, 1997.
- [17] M. M. Aggarwal et al. (WA98 Collaboration), hep-ex/9710015.

- [18] R. D. Amado and Y. Lu, Phys. Rev. D **54** (1996) 7075.
- [19] J. Randrup and R. L. Thews, Phys. Rev. D **56** (1997) 4392.
- [20] R. D. Amado and I. I. Kogan, Phys. Rev. D **51** (1995) 190.
- [21] S. Mrówczyński and B. Müller, Phys. Lett. **B363** (1995) 1.
- [22] H. Hiro-Oka and H. Minakata, TMUP-HEL-9714, hep-ph/9712476, Phys. Lett. B, to be published.
- [23] S. L. Adler, Phys. Rev. **177** (1969) 2426; J. S. Bell and R. Jackiw, Nuovo Cimento **60A** (1969) 47.
- [24] J. Wess and B. Zumino, Phys. Lett. **B37** (1971) 95; E. Witten, Nucl. Phys. **B223** (1983) 422.
- [25] H. Minakata and B. Müller, Phys. Lett. **B377** (1996) 135.
- [26] M. Asakawa, Z. Huang, and X. N. Wang, in preparation.
- [27] W. H. Press, S. A. Teukolsky, W. T. Vetterling, and B. P. Flannery, *Numerical Recipes* (Cambridge University Press, 1986).
- [28] W. H. Press, B. S. Ryden, and D. N. Spergel, Ap. J. **347** (1989) 590.
- [29] G. Dahlquist and Å. Björck, *Numerical Methods* (Prentice Hall, 1974).
- [30] Hereafter we denote the conjugate fields by $\dot{\phi}^i$ to avoid potential confusion.
- [31] Since the π_2 and π_3 fields are coupled in the equation of motion, if the time evolution of the π_3 field is changed, that of the π_2 field is changed as well. What we mean here is that the global behavior of the π_2 field, such as the size of the apparent domains and no existence of the upper-lower asymmetry, is not changed.
- [32] C. Itzykson and J.-B. Zuber, *Quantum Field Theory* (McGraw-Hill, New York, 1980).

- [33] M. Asakawa, H. Minakata, B. Müller, and K. Rajagopal, in preparation.
- [34] Z. Huang and X. N. Wang, *Phys. Rev. D* **49** (1994) R4335.
- [35] J. J. Sakurai, *Modern Quantum Mechanics* (Addison-Wesley, 1985).
- [36] see e.g.: D. L. Goodstein, *States of Matter*, Chap. 4 (Prentice-Hall, 1975).
- [37] J. W. Cahn, *J. Chem. Phys.* **42** (1964) 93.
- [38] Y. Oono and S. Puri, *Phys. Rev. A* **38** (1988) 434.

FIGURE CAPTIONS

Fig. 1: Example of initial $\dot{\pi}_3$ field configuration.

Fig. 2: Example of initial $\dot{\pi}_2$ field configuration.

Fig. 3: Example of initial $\dot{\pi}_3$ field configuration. The value of the kick has been artificially increased by a factor of five to $a_n = 0.5$.

Fig. 4: Proper time evolution of the π_3 field in an event.

Fig. 5: Proper time evolution of the π_2 field in an event.

Fig. 6: Fourier power of π_3 at $\tau = 4$ fm in an event.

Fig. 7: Fourier power of π_2 at $\tau = 4$ fm in an event.

Fig. 8: $\langle A_0^1 \rangle_{\text{upper}}$, $\langle A_0^3 \rangle_{\text{upper}}$, and $\langle A_0^3 \rangle_{\text{lower}}$ as a function of proper time. The average is taken over 10 events.

Fig. 9: $\langle V_0^1 \rangle_{\text{upper}}$, $\langle V_0^3 \rangle_{\text{upper}}$ as a function of proper time. The average is taken over 10 events.

Fig. 10: $\langle \pi_1 \rangle_{\text{upper}}$, $\langle \pi_3 \rangle_{\text{upper}}$, and $\langle \pi_3 \rangle_{\text{lower}}$ as a function of proper time. The average is taken over 10 events.

Fig. 11: $\langle A_0^1 \rangle_{\text{upper}}$, $\langle A_0^3 \rangle_{\text{upper}}$, and $\langle A_0^3 \rangle_{\text{lower}}$ as a function of proper time for the case with $R_0 = 5$ fm. The average is taken over 100 events.

Fig. 12: $A_{11}(r, \tau)$ at $\tau = 1, 5,$ and 9 fm. The average is taken over 5 events.

Fig. 13: $A_{33}^{++}(r, \tau)$ and $A_{33}^{+-}(r, \tau)$ at $\tau = 7$ and 9 fm. The average is taken over 5 events.

Fig. 14: $A_{11}^{++}(r, \tau)$ and $A_{11}^{+-}(r, \tau)$ at $\tau = 7$ fm. The average is taken over 5 events.

Fig. 15: $B_{33}^{++}(r, \tau)$ and $B_{33}^{+-}(r, \tau)$ at $\tau = 9$ fm. The average is taken over 5 events.

Fig. 16: $B_{11}^{++}(r, \tau)$, $C_{11}^{++}(r, \tau)$, and $C_{33}^{++}(r, \tau)$ at $\tau = 9$ fm. The average is taken over 5 events.

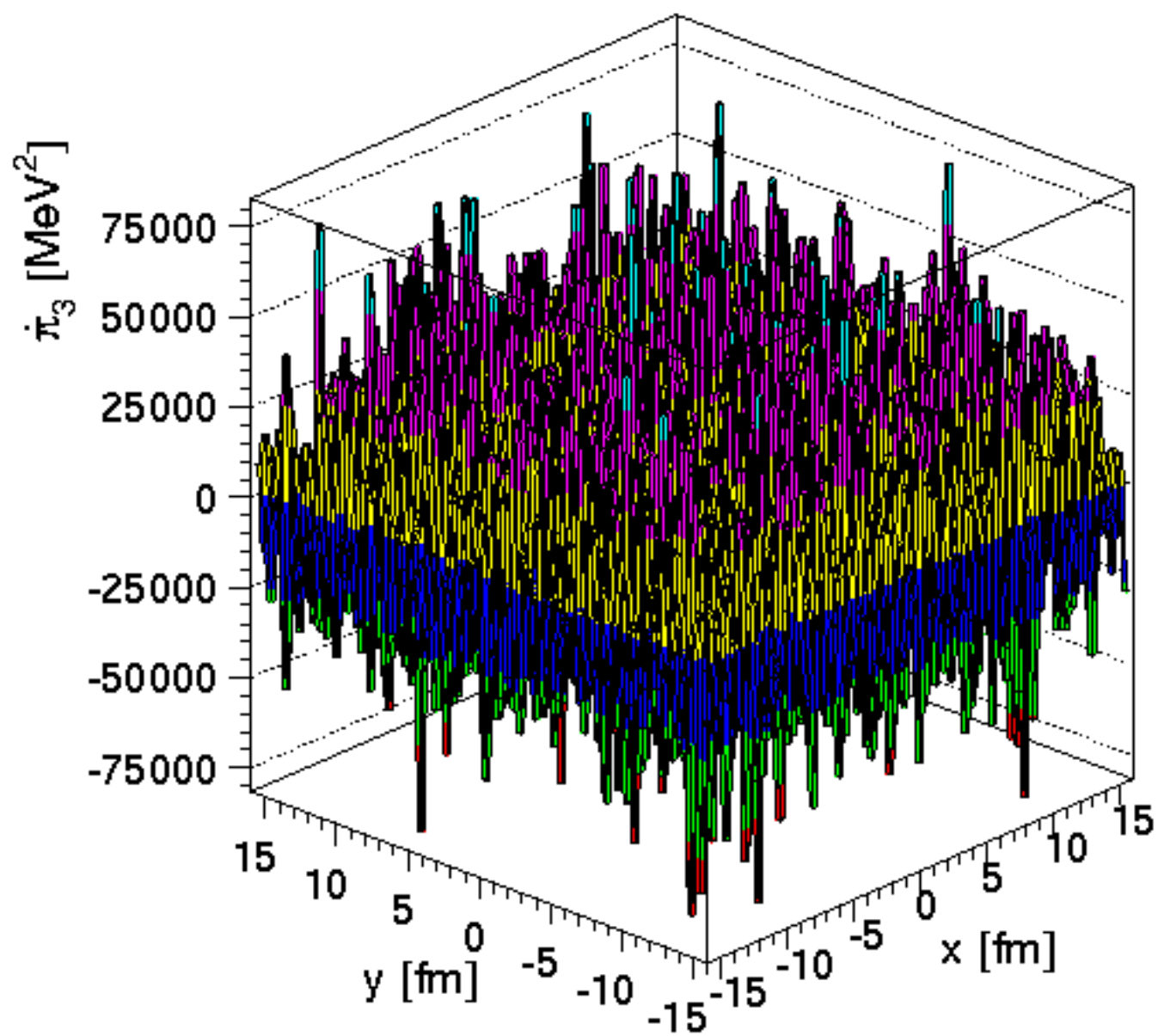
Fig. 17: Proper time evolution of the distribution of π^0 density in an event.

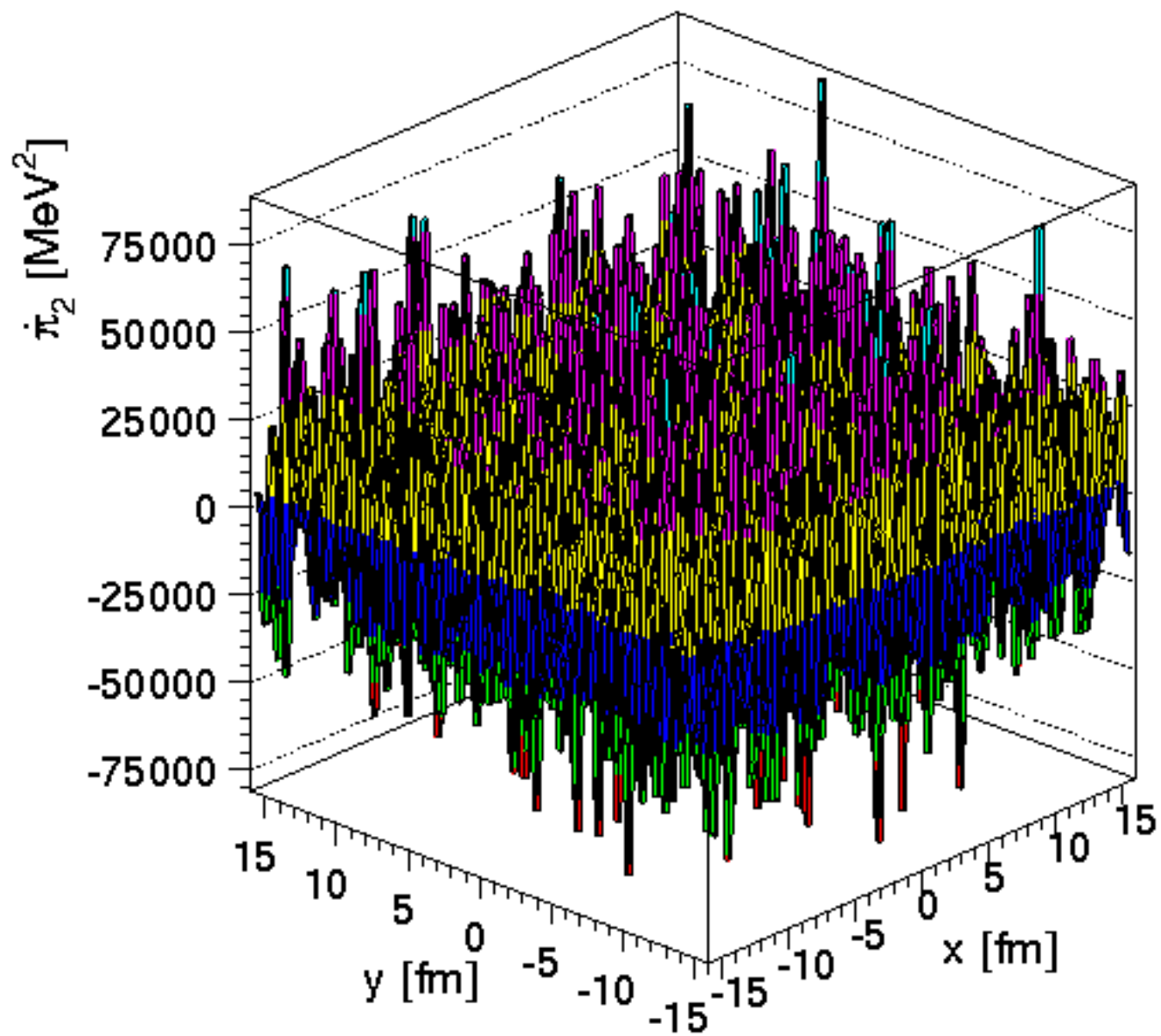
Fig. 18: Proper time evolution of the distribution of π^+ density in an event.

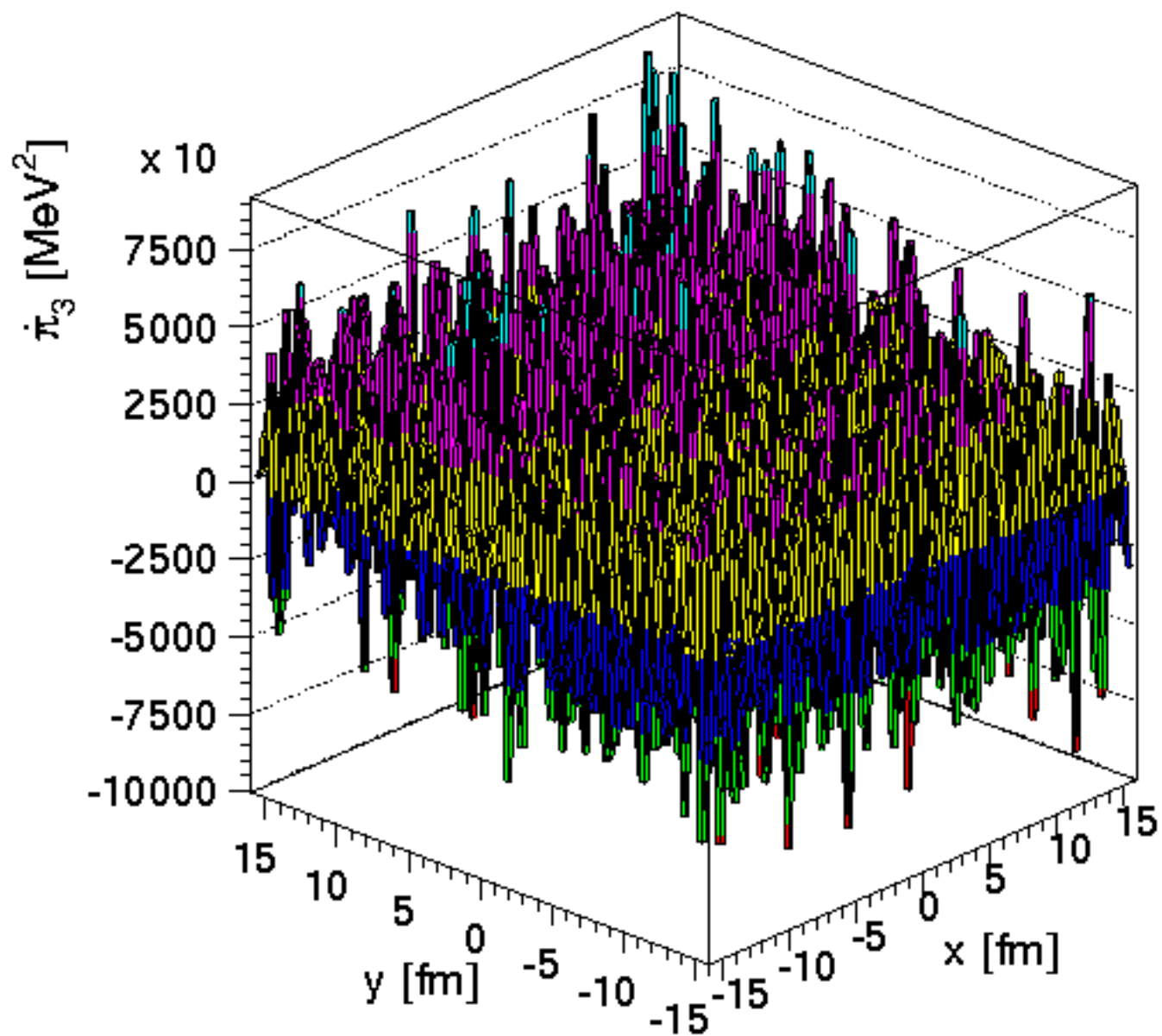
Fig. 19: Proper time evolution of the distribution of $R(\vec{x})$.

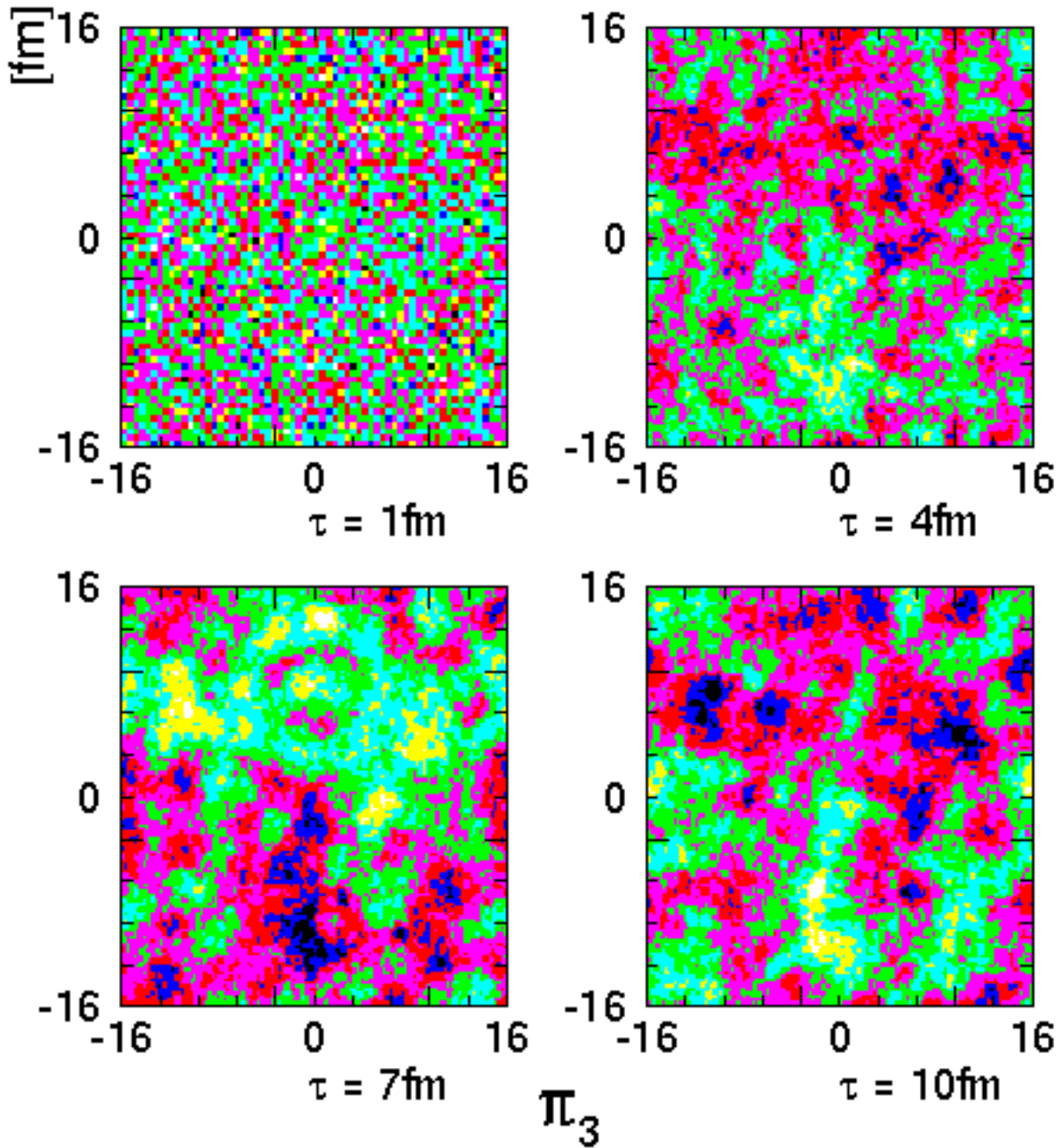
Fig. 20: Solid line is the proper time evolution of R averaged over 10 events. The dashed line is the same except that the momentum integration is limited to $k < 250$ MeV.

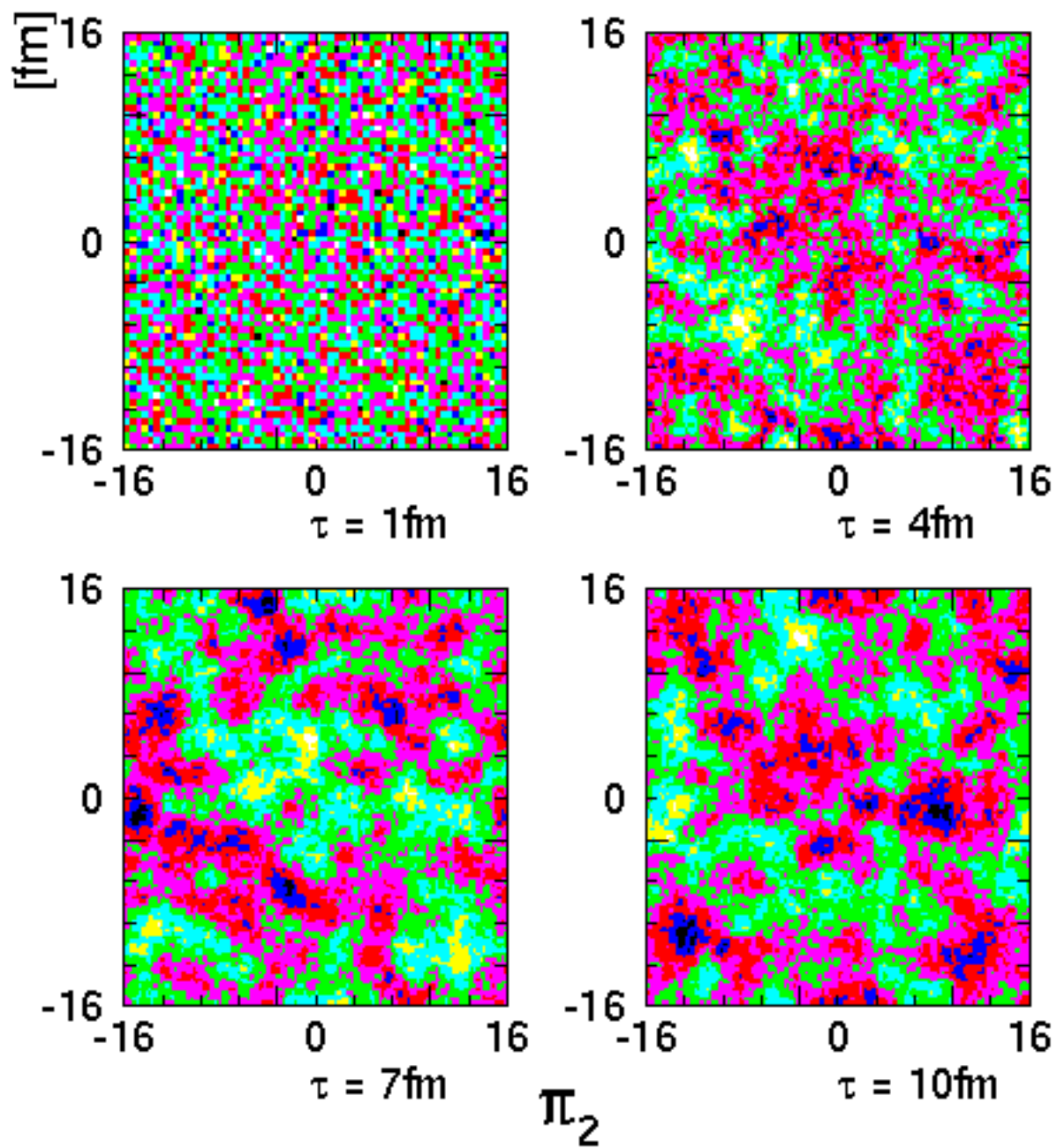
Fig. 21: Same as Fig. 20 except that no anomaly kick is exerted.

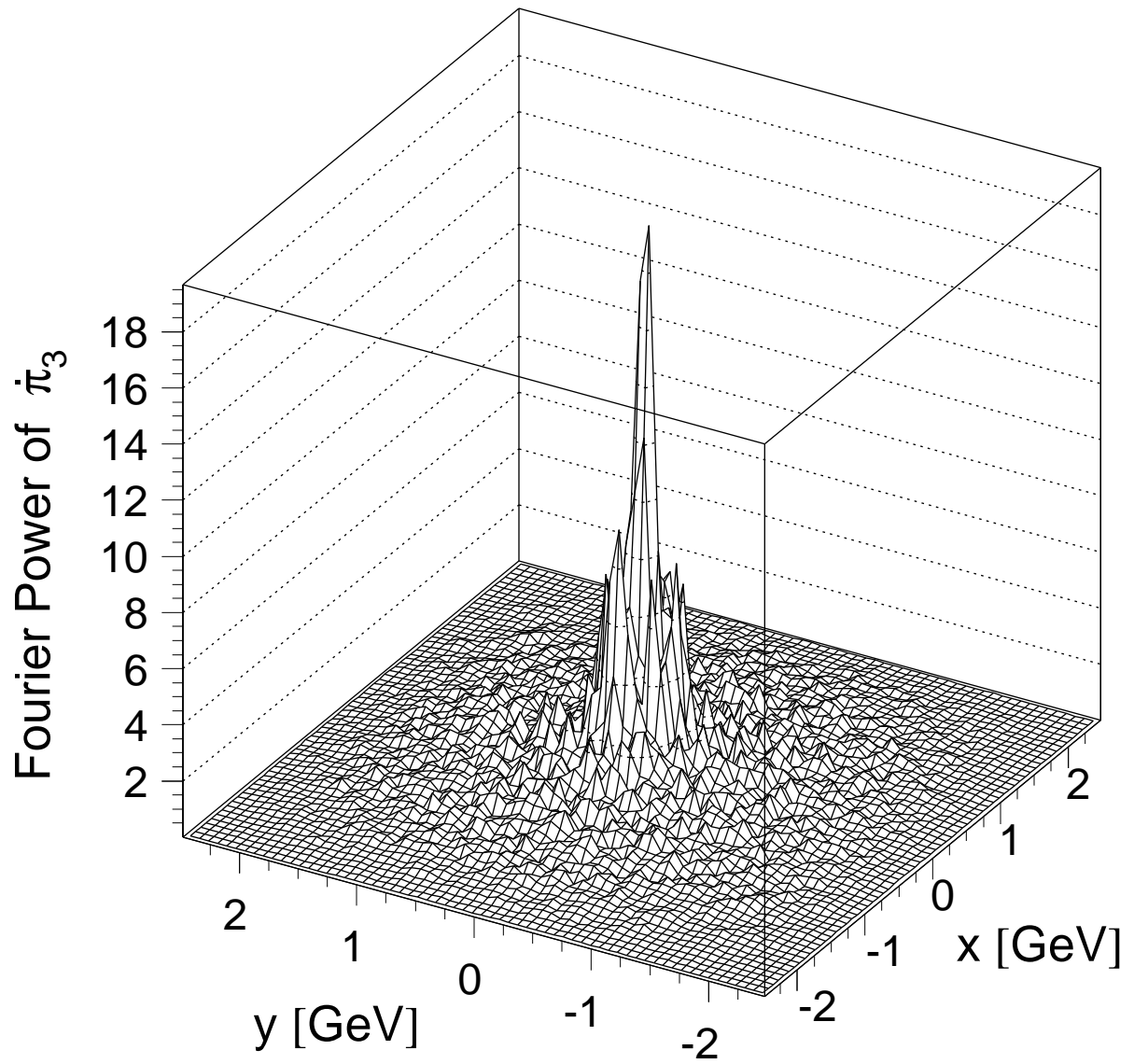


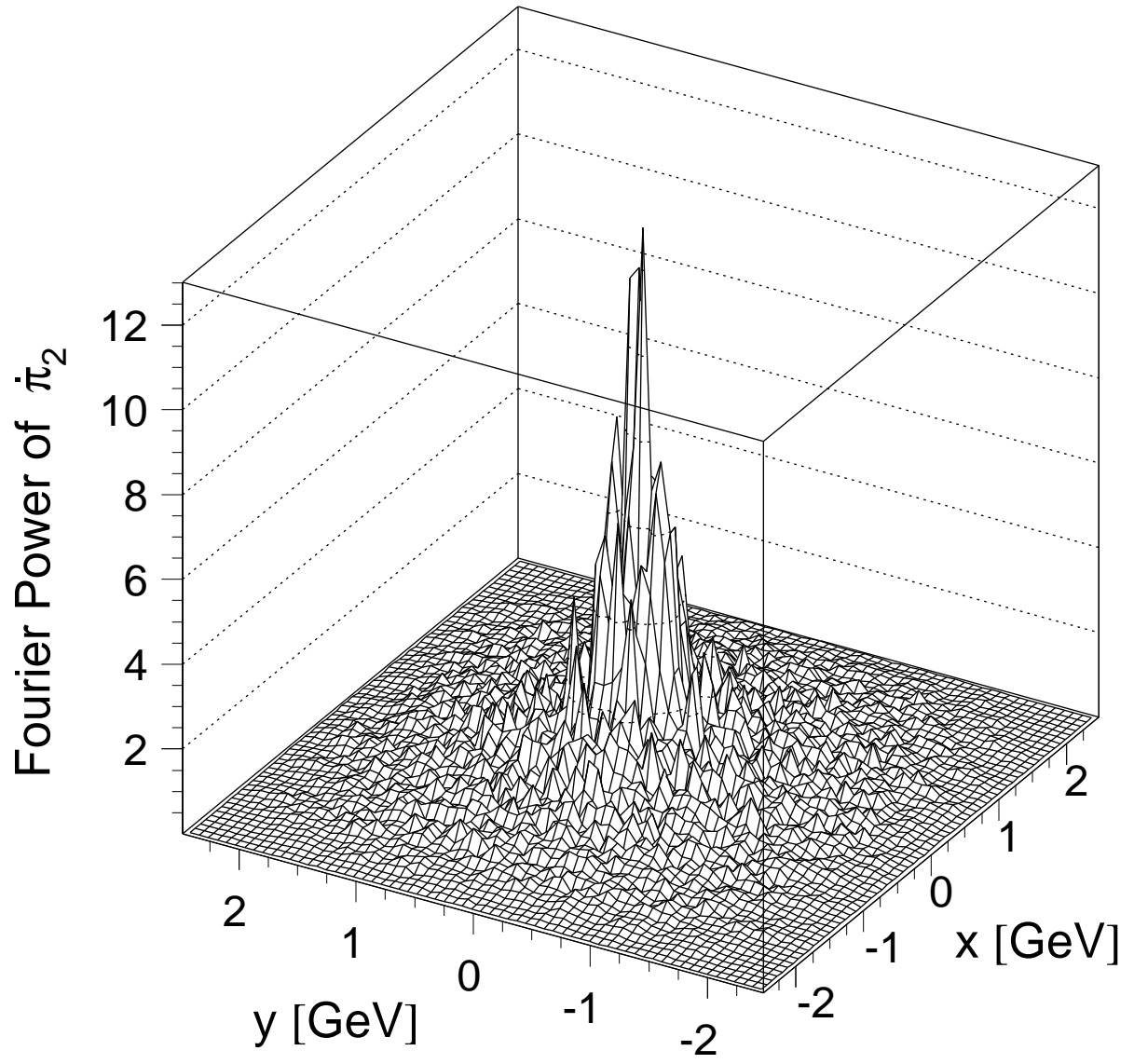


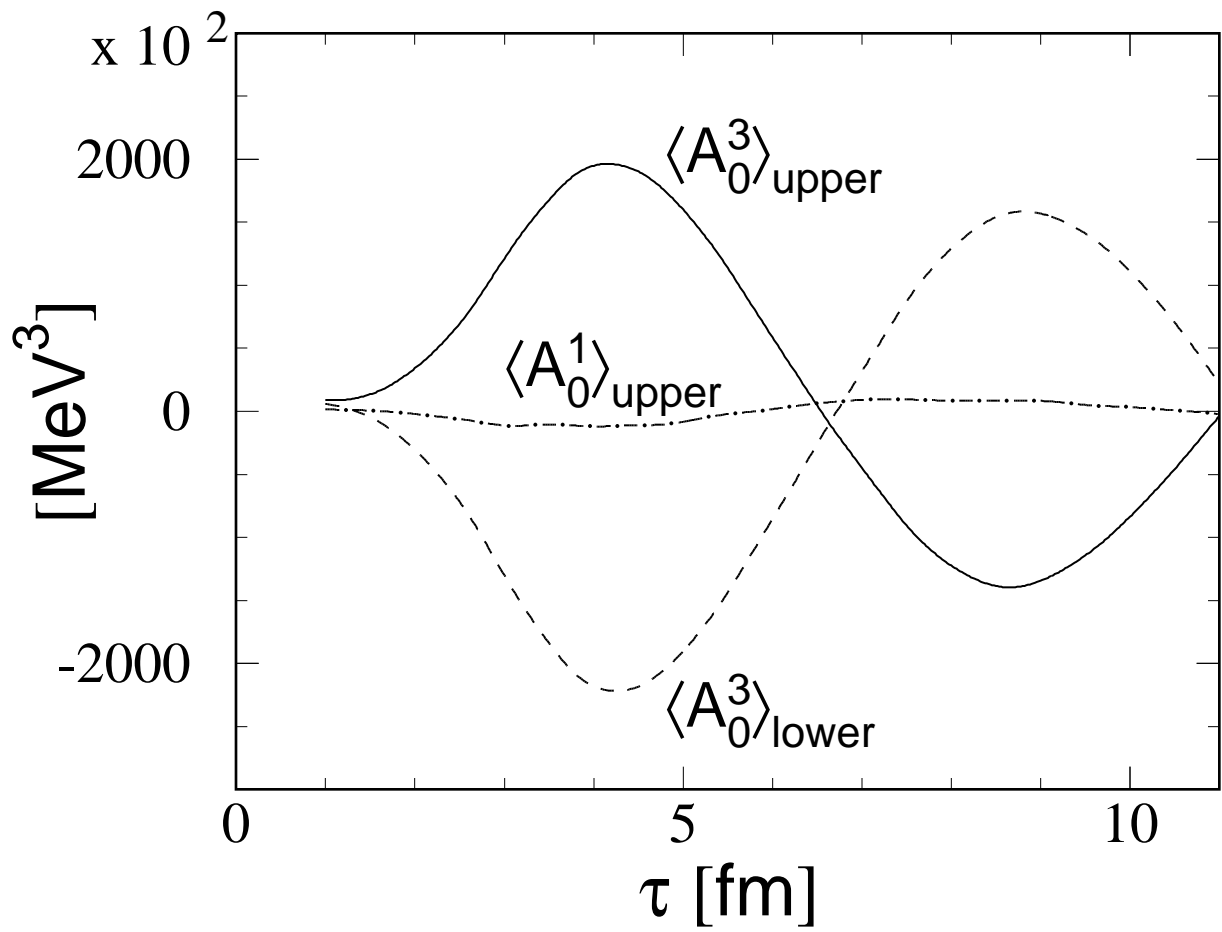


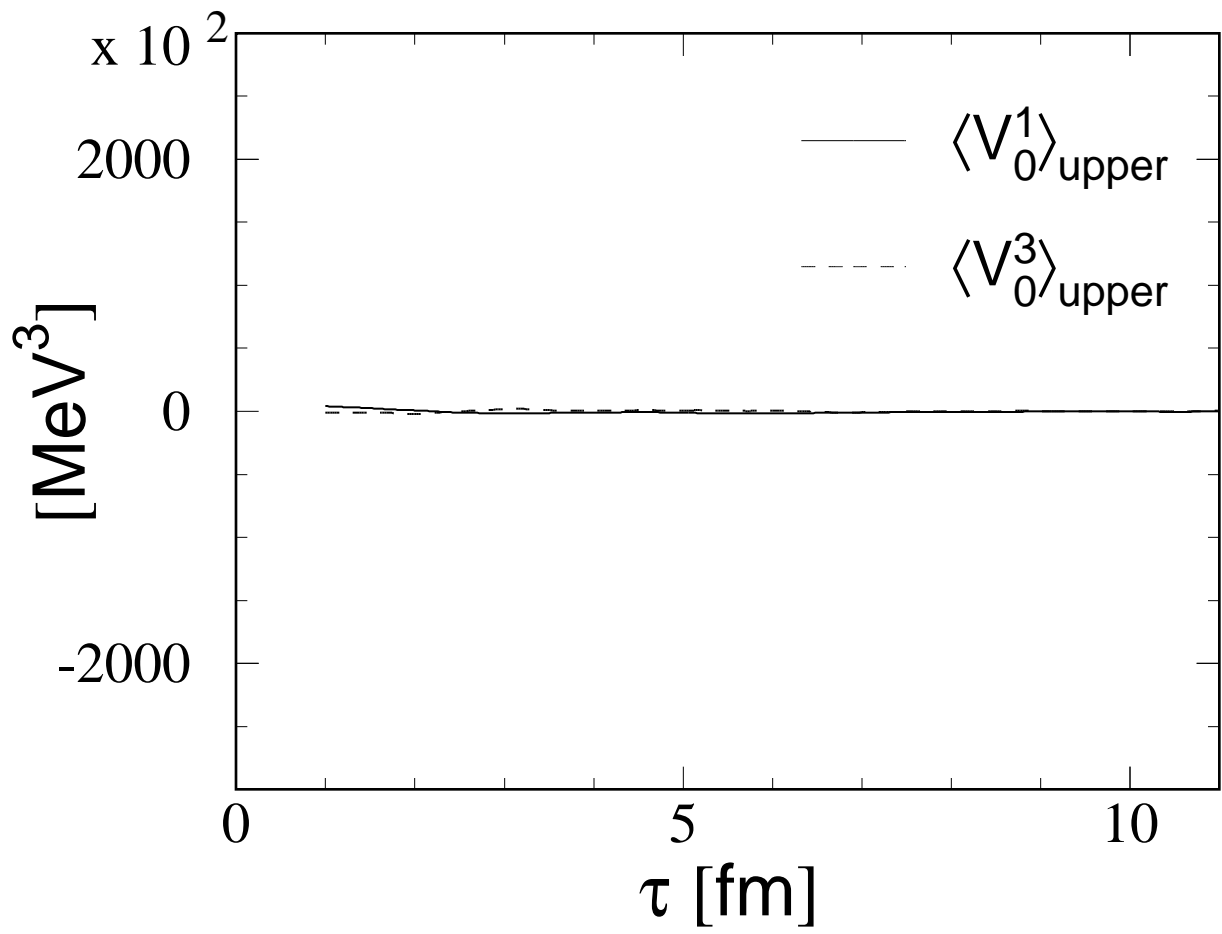


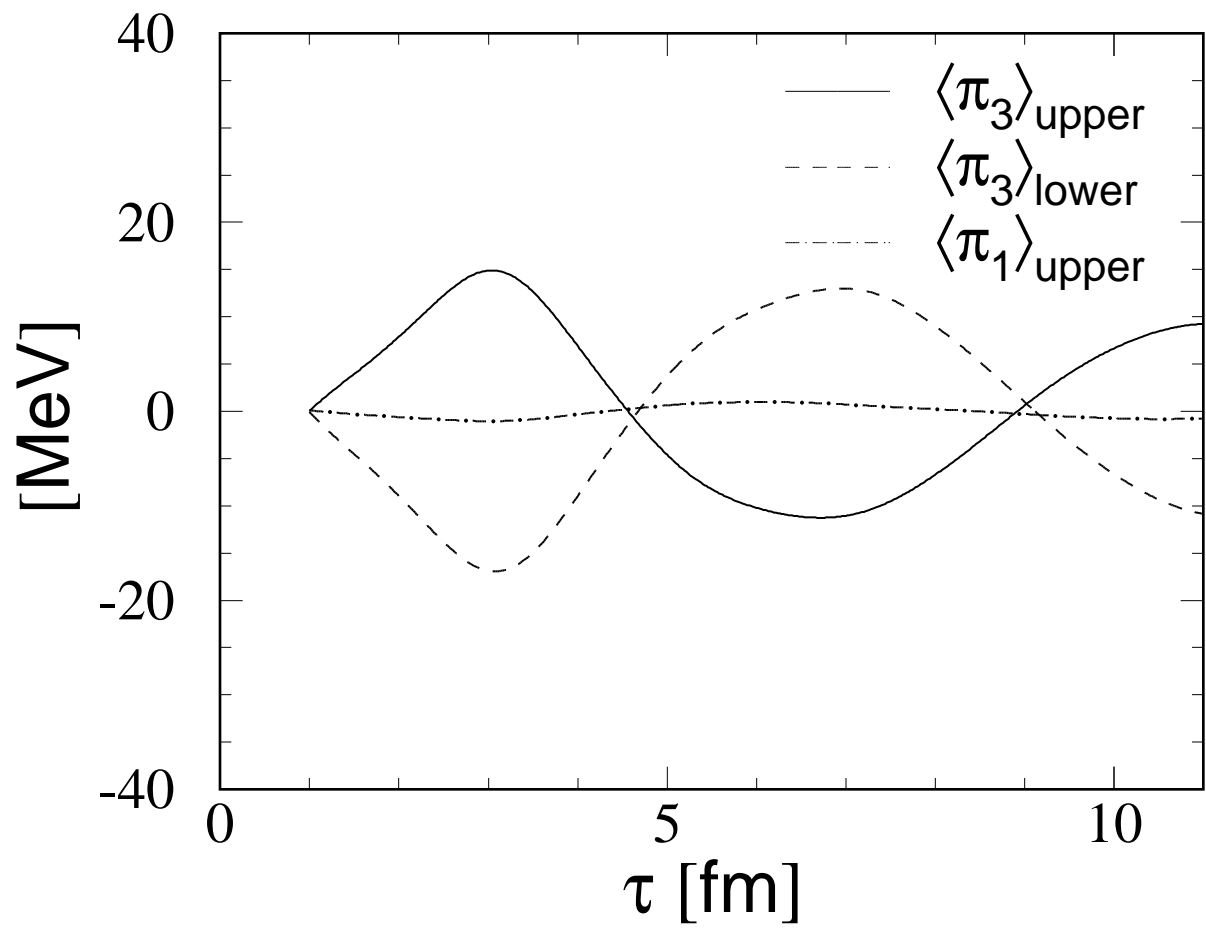


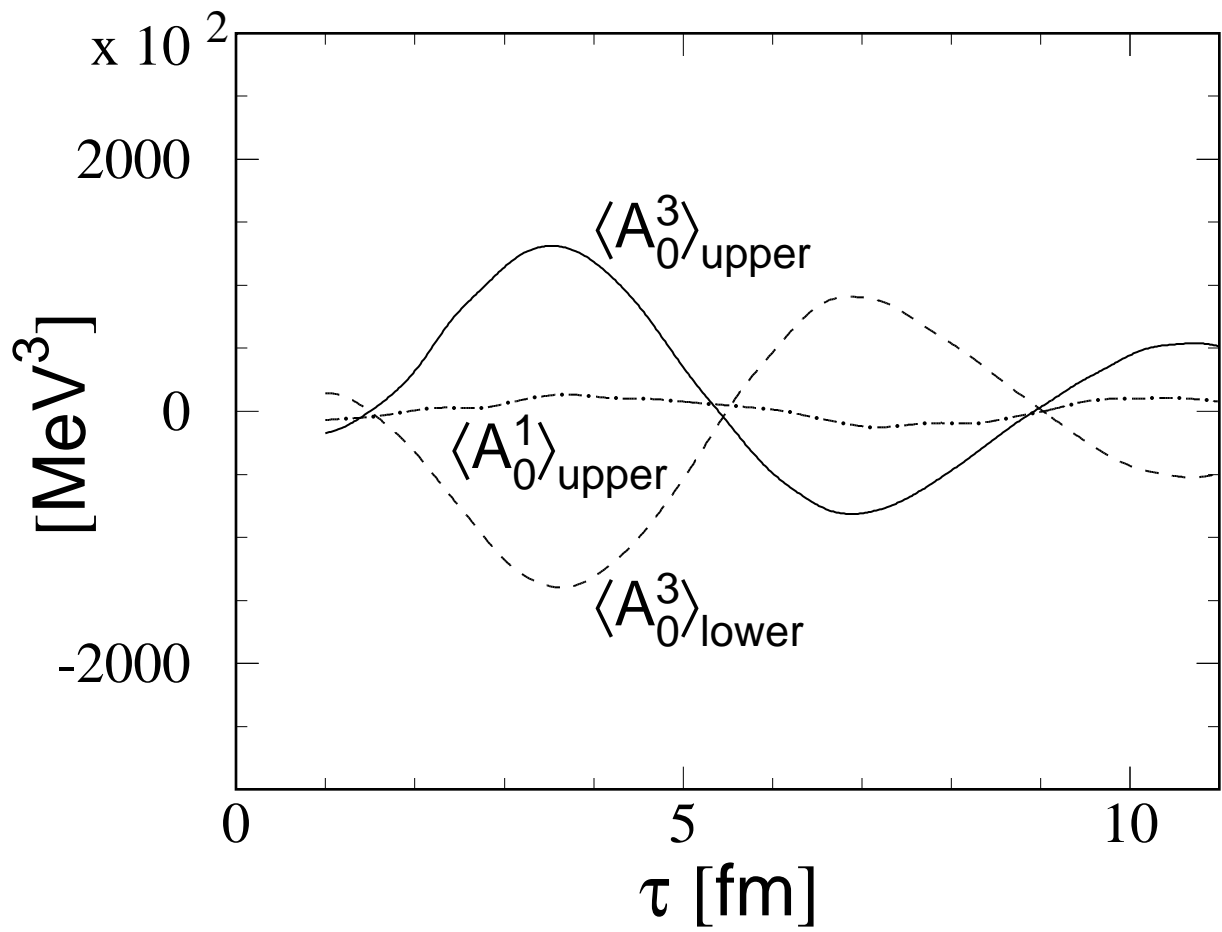


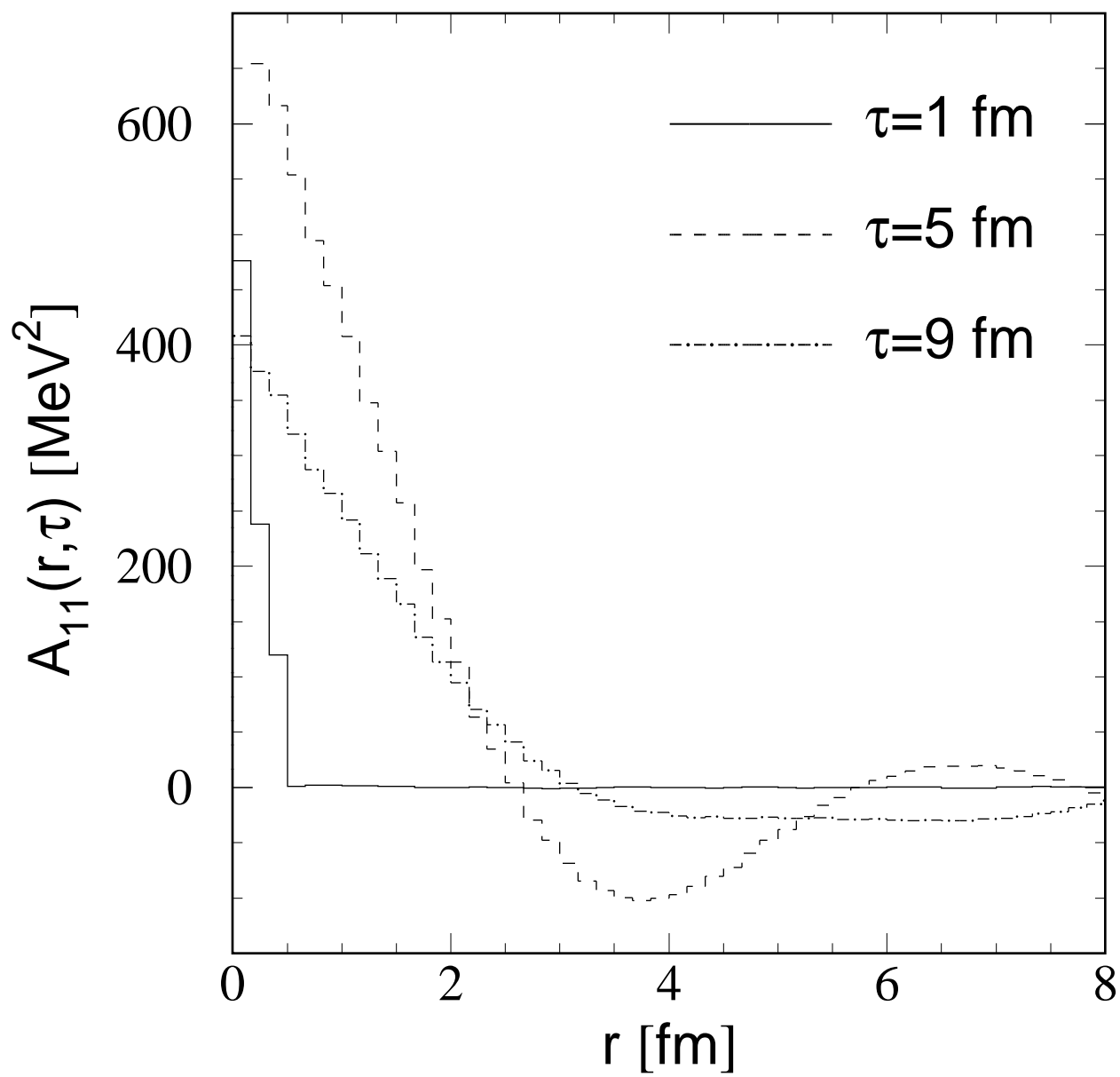


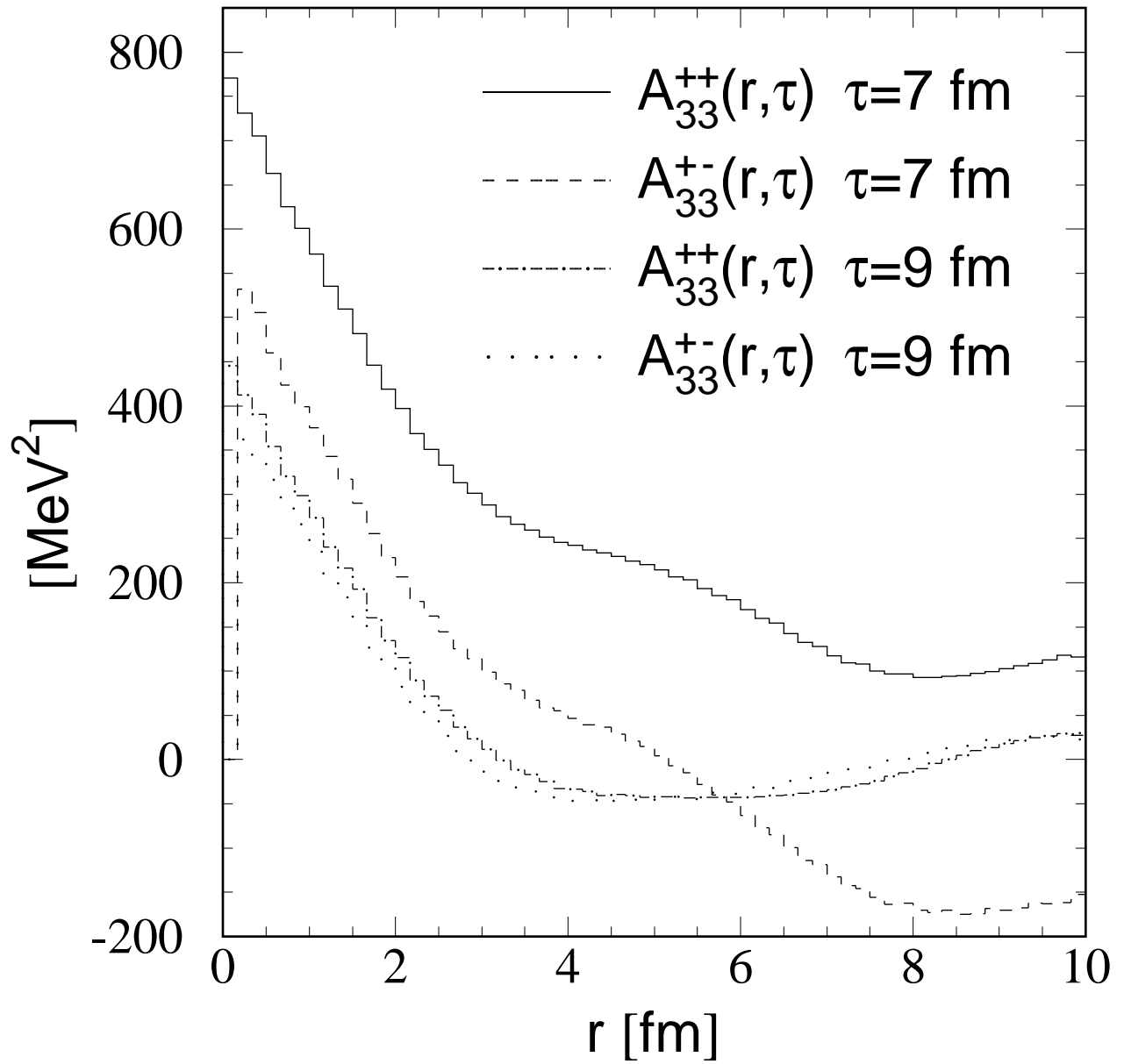


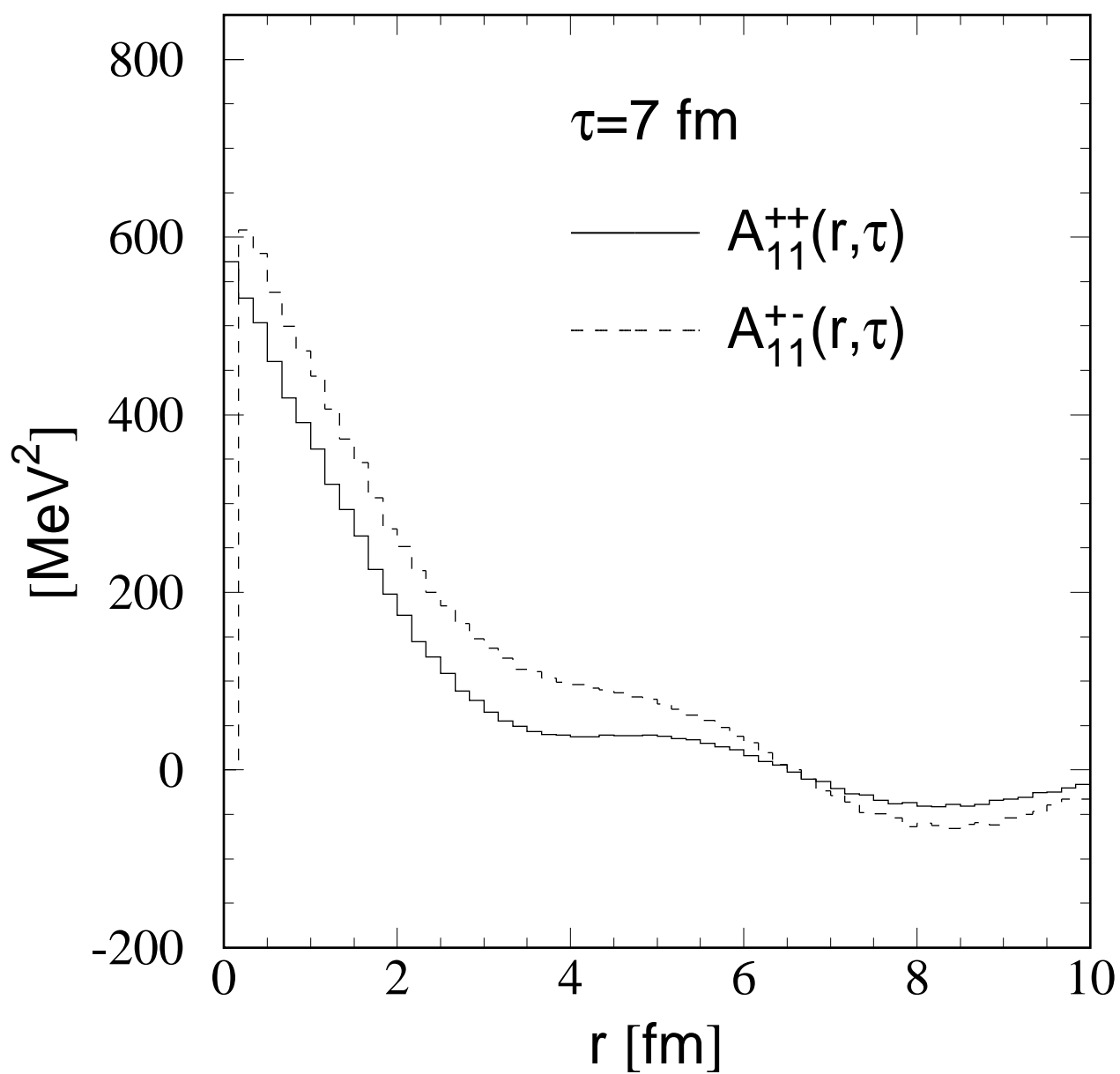


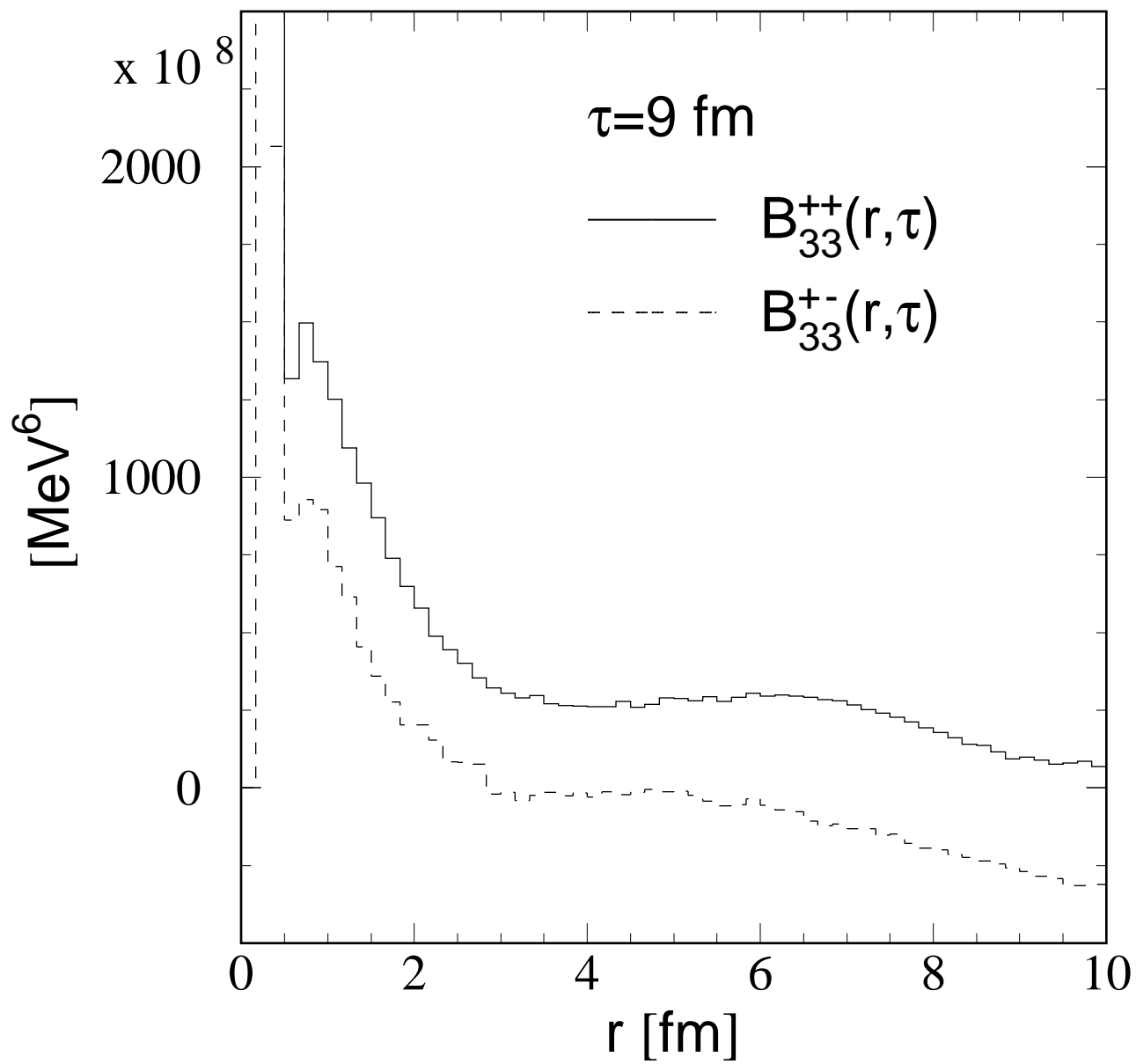


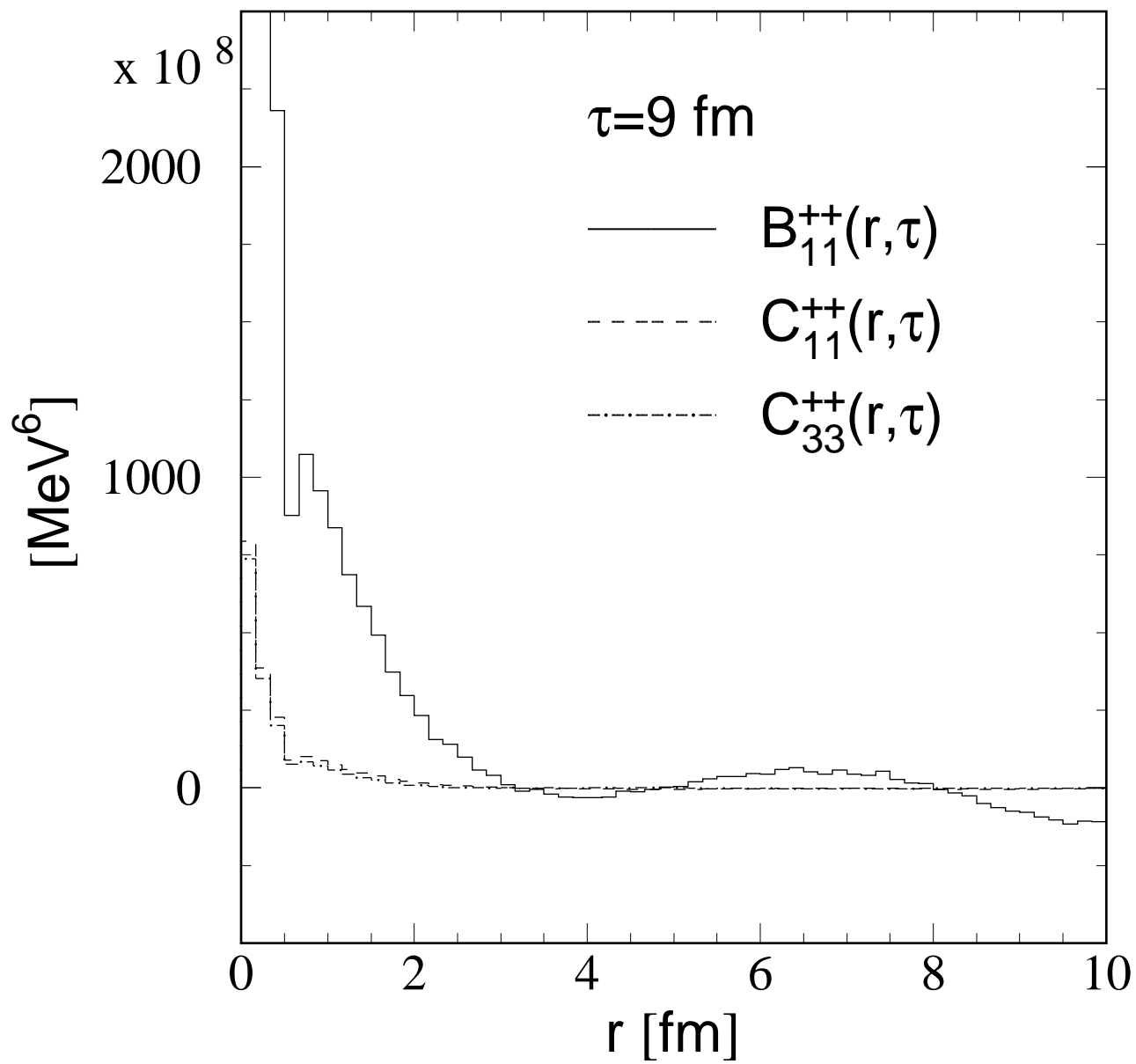


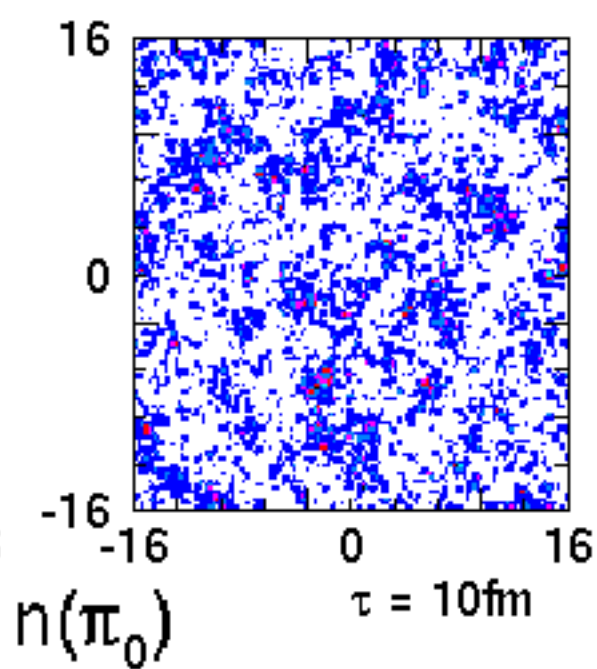
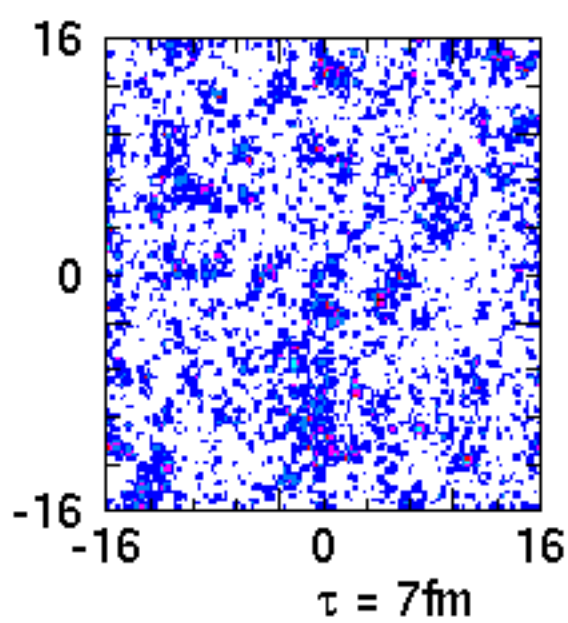
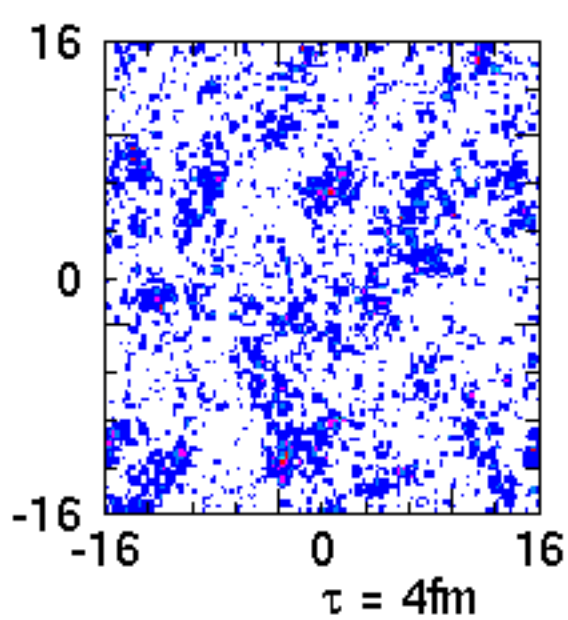
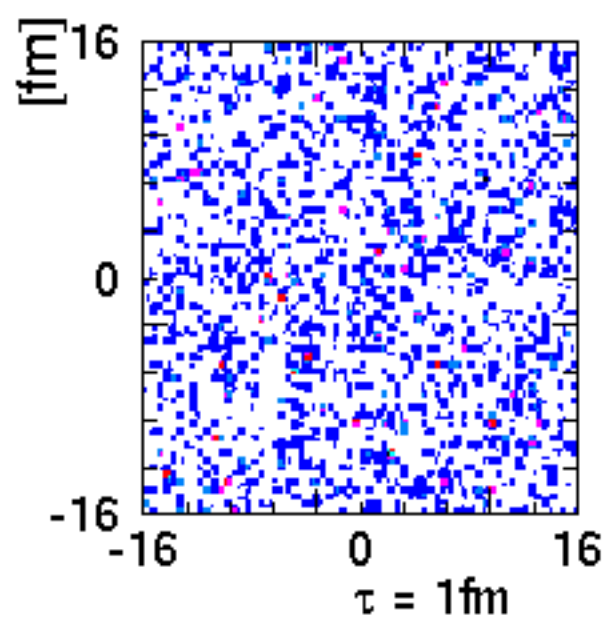












$n(\pi_0)$

